Numerical Solutions of the Linearized Euler Equations for Unsteady Vortical Flows Around Lifting Airfoils

James R. Scott
Lewis Research Center
Cleveland, Ohio

and

Hafiz M. Atassi
University of Notre Dame
Notre Dame, Indiana

NASA

NUMERICAL SOLUTIONS OF THE LINEARIZED EULER EQUATIONS FOR UNSTEADY VORTICAL FLOWS AROUND LIFTING AIRFOILS

James R. Scott*
NASA Lewis Research Center
Cleveland, OH 44135

Hafiz M. Atassi**
University of Notre Dame
Notre Dame, IN 46556

Abstract

A linearized unsteady aerodynamic analysis is presented for unsteady, subsonic vortical flows around lifting airfoils. The analysis fully accounts for the distortion effects of the nonuniform mean flow on the imposed vortical disturbances. A frequency domain numerical scheme which implements this linearized approach is described, and numerical results are presented for a large variety of flow configurations. The results demonstrate the effects of airfoil thickness, angle of attack, camber, and Mach number on the unsteady lift and moment of airfoils subjected to periodic vortical gusts. The results show that mean flow distortion can have a very strong effect on the airfoil unsteady response, and that the effect depends strongly upon the reduced frequency, Mach number, and gust wave numbers.

I. Introduction

Aerodynamicists have been concerned with the analysis of unsteady flows since the early days of powered flight. Vibration problems and flutter were the main concerns of early researchers. Because of the complexity of unsteady flows, and due to the lack of computational capabilities, the classical work in unsteady aerodynamics relied heavily upon mathematical analysis and engineering approximations. The first treatments which analyzed the unsteady flow around an oscillating airfoil assumed the blade to be a simple flat plate airfoil in incompressible flow. By assuming the airfoil to be a flat plate at zero mean incidence, the early researchers were able to linearize the governing equations about a uniform mean flow and to uncouple the unsteady part of the flow from the uniform steady state.

Later work in unsteady aerodynamics was concerned with predicting unsteady gust loading on airfoils due to the occurrence of upstream vortical disturbances and flow nonuniformities. The main engineering problems which mo-

---

* Research Scientist
  Member AIAA

** Professor, Aerospace and Mechanical Engineering
   Associate Fellow, AIAA

tivated this concern were the effects of atmospheric turbulence on aircraft wings and the effects of upstream flow nonuniformities on rotating propeller blades. By using the thin airfoil approximation and decomposing the unsteady velocity into solenoidal and irrotational (potential) components, the early researchers were able to reduce the mathematical formulation of the gust response problem to essentially that of the oscillating airfoil problem. Sears [1] was the first to derive an analytical solution for the unsteady lift on a rigid flat plate airfoil moving through a sinusoidal gust pattern in an incompressible flow.

In the 1960's and 70's, researchers began tackling the more general problem of unsteady flows around lifting airfoils. The theoretical analysis of the unsteady flow in this case is much more difficult than for the case of thin, unloaded airfoils. For the lifting airfoil problem the mean flow is no longer uniform and the unsteady flow cannot be uncoupled from the steady mean flow.

Goldstein and Atassi [2] were the first to present a theoretical treatment of unsteady vortical flow around lifting airfoils that fully accounts for the coupling between the steady mean flow and the unsteady perturbation velocity field. Their second-order analysis of two-dimensional, incompressible, periodic vortical flows around thin airfoils with small camber and angle of attack showed that the convected vortical gusts are nonlinearly distorted by the spatially varying mean flow.

The problem was re-examined by Atassi [3], who showed that in spite of the nonlinear character of the interactive gust problem, the unsteady lift formula can be written as the sum of the Sears function and three other functions accounting separately for the effects of mean flow incidence, airfoil camber, and airfoil thickness. The explicit formulas for the unsteady lift derived in [2] and [3] showed that for a transverse and longitudinal gust, the mean flow distortion has a very strong effect on the magnitude and phase of the gust response.

For most flows encountered in applications, one deals with heavily loaded airfoils at high Mach number and with three-dimensional upstream gusts. The formulation for the unsteady gust problem in this case leads to the linearized Euler equations. Goldstein [4] presented an approach for this general problem in which he split the unsteady velocity field into vortical and potential parts. The vortical part

is determined from the gust upstream conditions and the Lagrangian coordinates of the mean flow, and the potential part is governed by a non-constant coefficient, inhomogeneous convective wave equation. Thus in Goldstein's formulation, the mathematical problem is reduced to solving a single equation. Goldstein's work thus brought about a significant simplification in the formulation of unsteady vortical flows.

For the important special case of flows past a body with a stagnation point, however, Goldstein's vortical velocity becomes singular along the body surface and in the wake. Due to this singularity in the vortical velocity, the unknown potential must satisfy singular boundary conditions along these surfaces. These features make it difficult to use Goldstein's approach directly for numerical computations of unsteady vortical flows past a body with a stagnation point.

Atassi and Grzedzinski [5] have shown that it is possible to modify Goldstein's splitting of the unsteady velocity in such a way as to remove the singularity in the vortical velocity along the body surface and in the wake. Their regularization of Goldstein's approach leads to a formulation for the unsteady problem which is well-suited to numerical solution techniques.

Up until recently, most numerical work in unsteady aerodynamics concentrated on potential methods. The early work dealt with solving the unsteady small disturbance potential equation as a way of obtaining the unsteady flow around oscillating airfoils or cascades. Later work was directed toward solving the linearized unsteady potential equation and the unsteady full potential equation. More recently researchers have worked to develop the so-called primitive variable methods, wherein the full unsteady Euler or Navier-Stokes equations are solved using a time-marching approach. Whereas the earlier potential methods were directed primarily at solving unsteady flows around oscillating airfoils and cascades, the primitive variable approach can be used to solve a wider range of unsteady flows. This approach, however, has the drawback of being prohibitively expensive for routine engineering calculations such as are encountered in design work.

In the present paper we are concerned with large scale unsteady disturbances such as are encountered in the rotor-stator interaction of turbomachinery and propellers. For such flows the length scale associated with the upstream vortical disturbances is usually of the same order of magnitude as the blade chord, and the characteristic unsteady velocity is in many applications an order of magnitude less than the mean velocity. Thus, if we denote the length scale by l' and the characteristic velocity by $|\vec{u}_\infty|$, the time scale associated with the upstream unsteady disturbances is $\frac{l'}{|\vec{u}_\infty|}$. The time scale associated with the underlying mean flow is $\frac{c}{U_{\infty,rel}}$, where c is the airfoil chord length and $U_{\infty,rel}$ is the relative mean velocity. Then for large scale upstream disturbances where l' is the same order of magnitude as the blade chord or larger, and $|\vec{u}_\infty|$ is small compared to $U_{\infty,rel}$, we will have

$$\frac{c}{U_{\infty,rel}} \ll \frac{l'}{|\vec{u}_\infty|}. \qquad (1.1)$$

That is, the time scale associated with the mean flow is an order of magnitude less than the time scale associated with the upstream unsteady disturbances. This is essentially the condition under which the linearized approach is valid.

For this kind of unsteady flow, the dominant effects will be due to the high speed convection of the upstream flow nonuniformities, and the linearized aerodynamic approach of Goldstein as modified by Atassi and Grzedzinski represents an attractive alternative to the primitive variable approach.

The authors have developed a finite difference, frequency domain numerical scheme which implements this linearized approach for the purpose of obtaining numerical solutions to compressible, unsteady, periodic vortical flows around two-dimensional lifting airfoils. The scheme that we present fully accounts for the distortion of the imposed upstream vortical disturbances by the nonuniform mean flow. Previous numerical efforts by McCroskey and Goorjian [6] and McCroskey [7] to solve this kind of unsteady vortical flow have not accounted for the distortion of the imposed gust by the mean flow gradients, but have invoked the linear thin airfoil approximation in which the gust propagates without distortion. As was shown in [2] and [3], and as will be seen later in the present paper, the mean flow distortion has a very strong effect on the airfoil unsteady response, and must be taken into account if accurate unsteady results are to be obtained.

From a computational standpoint, there are numerous advantages to the numerical scheme which we have developed. Among the advantages are the fact that the requirements for CPU time and computer storage are much less than for primitive variable methods. The codes that have been developed can easily be run on a present day scientific work station as opposed to requiring a large mainframe computer. In addition, since the governing equation is linear, a variety of standard differencing schemes are available for the numerical solution of the boundary value problem, and the derivation of physically correct far field boundary conditions is much simpler.

Another advantage of the present approach is that it provides not only an accurate near field solution from which the body dynamic response to the imposed vortical disturbance can be determined, but it also provides an accurate far field solution from which the acoustic radiation can be calculated. This will directly yield the acoustic intensity and power radiated without the use of Lighthill's analogy and the tedious calculation which may result from the refraction and scattering of the radiated acoustic waves by the spatially varying flow field.

Our major purpose in the present paper is to present numerical solutions for the general problem of unsteady vortical flows around lifting airfoils in compressible subsonic flows. The results that are presented demonstrate the effects of airfoil thickness, camber, angle of attack, and Mach

number on the airfoil unsteady response (unsteady lift and moment) to three-dimensional, periodic vortical gusts imposed upstream. In Section II, we present the mathematical formulation of the general boundary value problem. In Section III, we give a brief description of the numerical scheme that has been developed. Readers interested in the full details of our numerical approach should consult References 8 or 9. Finally, in Section IV we present and discuss numerical results for a large variety of flow configurations.

II. Linearized Unsteady Aerodynamics for Nonuniform Potential Flow Fields

Linearized Euler Equations

Consider an inviscid, compressible flow past an airfoil placed at nonzero incidence to a stream with uniform upstream velocity U_∞ in the x_1 direction. We shall assume in the present discussion that there are no shocks in the flow. Now if we also assume the fluid to be an ideal, non-heat conducting gas with constant specific heats, then the governing continuity, momentum, and energy equations can be written

$$\frac{D\rho}{Dt} + \rho\vec{\nabla} \cdot \vec{U} = 0 \qquad (2.1)$$

$$\rho\frac{D\vec{U}}{Dt} = -\vec{\nabla}p \qquad (2.2)$$

$$\frac{Ds}{Dt} = 0 \qquad (2.3)$$

where $\frac{D}{Dt}$ is the material derivative.

In the absence of upstream flow disturbances, and assuming the airfoil to be rigid, there will be a steady flow $\vec{U}_0(\vec{x})$ about the airfoil such that $\vec{U}_0(\vec{x}) \to U_\infty\vec{i}$ as $x_1 \to -\infty$, where $\vec{i}$ is a unit vector in the x_1 direction. Let us suppose that far upstream a small amplitude, unsteady velocity disturbance, which we will denote by $\vec{u}_\infty$, is imposed on the flow. Then since $|\vec{u}_\infty|$ is small compared to U_∞, we assume that there will be small, unsteady perturbations in the physical properties of the otherwise steady flow. It is therefore reasonable to linearize the governing equations (2.1) - (2.3) about the mean flow state and to introduce perturbation quantities as follows:

$$\vec{U}(\vec{x},t) = \vec{U}_0(\vec{x}) + \vec{u}(\vec{x},t) \qquad (2.4)$$

$$p(\vec{x},t) = p_0(\vec{x}) + p'(\vec{x},t) \qquad (2.5)$$

$$\rho(\vec{x},t) = \rho_0(\vec{x}) + \rho'(\vec{x},t) \qquad (2.6)$$

$$s(\vec{x},t) = s_0 + s'(\vec{x},t) \qquad (2.7)$$

where 0 subscripts denote the steady mean flow quantities which are assumed to be known, the entropy s_0 is constant, and $\vec{u}$, p', ρ', and s' are the unsteady perturbation velocity, pressure, density and entropy, respectively.

Substituting relations (2.4) - (2.7) into equations (2.1) - (2.3) and neglecting products of small quantities, one obtains the following linearized continuity, momentum, and energy equations

$$\frac{D_0\rho'}{Dt} + \rho'\vec{\nabla} \cdot \vec{U}_0 + \vec{\nabla} \cdot (\rho_0\vec{u}) = 0 \qquad (2.8)$$

$$\rho_0(\frac{D_0\vec{u}}{Dt} + \vec{u} \cdot \vec{\nabla}\vec{U}_0) + \rho'\vec{U}_0 \cdot \vec{\nabla}\vec{U}_0 = -\vec{\nabla}p' \qquad (2.9)$$

$$\frac{D_0s'}{Dt} = 0, \qquad (2.10)$$

where $\frac{D_0}{Dt} = \frac{\partial}{\partial t} + \vec{U}_0 \cdot \vec{\nabla}$ is the convective derivative associated with the mean flow.

Equations (2.8) - (2.10) are the governing partial differential equations for the unknown perturbation quantities $\vec{u}, p', \rho'$, and s' for the problem of small, unsteady disturbances to an otherwise steady flow. The upstream disturbance $\vec{u}_\infty$ is essentially a boundary condition which is imposed on the unsteady velocity $\vec{u}$. That is, we must have $\vec{u} \to \vec{u}_\infty$ as $x_1 \to -\infty$. We shall assume in the present paper that $\vec{u}_\infty$ is the only upstream disturbance imposed on the mean flow, i.e., there are no imposed entropy disturbances or incident acoustic waves. Now from previous work concerning small amplitude velocity disturbances imposed on a uniform flow, it is known that the unsteady velocity can be decomposed into the sum of a vortical component which has zero divergence, is purely convected, and is decoupled from the pressure and any thermodynamic property, and an irrotational component which is directly related to the pressure but produces no entropy fluctuations [10,4] Then far upstream the total velocity $\vec{U}$ must be of the form

$$\vec{U} = U_\infty\vec{i} + \vec{u}_\infty(\vec{x} - \vec{i}U_\infty t) \qquad (2.11)$$

where

$$\vec{\nabla} \cdot \vec{u}_\infty = 0. \qquad (2.12)$$

There is no pressure associated with the velocity field $\vec{u}_\infty$. The unsteady velocity $\vec{u}$ must satisfy

$$\vec{u}(\vec{x},t) \to \vec{u}_\infty(\vec{x} - \vec{i}U_\infty t) \quad \text{as} \quad x_1 \to -\infty, \qquad (2.13)$$

and the pressure p' obeys

$$p'(\vec{x},t) \to 0 \quad \text{as} \quad x_1 \to -\infty. \qquad (2.14)$$

Goldstein's Approach

Goldstein [4] proposed a general approach for the analysis of potential mean flows with imposed upstream vortical and entropic disturbances which greatly simplifies the mathematical treatments of such flows. Under the conditions assumed on the flow in the previous section, the mean flow can be expressed as the gradient of a potential,

$$\vec{U}_0(\vec{x}) = \vec{\nabla}\Phi_0. \qquad (2.15)$$

In the present work we consider two-dimensional mean flow, so that $\vec{U}_0(\vec{x}) = (\frac{\partial\Phi_0}{\partial x_1}, \frac{\partial\Phi_0}{\partial x_2})$.

The simplest case of potential mean flow with imposed upstream disturbances is the thin airfoil problem where the potential flow is simply a uniform parallel flow. In this case it is advantageous to split the unsteady velocity into

a vortical component which is solenoidal, and an irrotational component which is expressed as the gradient of an unsteady potential. For the general problem of nonuniform flows around real airfoils, however, the splitting into solenoidal and irrotational components does not lead to any simplification of the mathematical formulation (See Reference 11 for details).

Goldstein proposed a new approach wherein the unsteady velocity is decomposed into the sum of a known vortical component $\vec{u}^{(I)}$ and an unknown potential component $\vec{\nabla}\phi$ so that

$$\vec{u}(\vec{x}, t) = \vec{u}^{(I)} + \vec{\nabla}\phi. \qquad (2.16)$$

The vortical component $\vec{u}^{(I)}$ is essentially a function of the upstream disturbance $\vec{u}_\infty$ and the mean flow Lagrangian coordinates and their spatial gradients. The unsteady potential satisfies a nonconstant-coefficient, inhomogeneous, convective wave equation

$$\frac{D_0}{Dt}\left(\frac{1}{c_0^2}\frac{D_0\phi}{Dt}\right) - \frac{1}{\rho_0}\vec{\nabla}\cdot(\rho_0\vec{\nabla}\phi) = \frac{1}{\rho_0}\vec{\nabla}\cdot(\rho_0\vec{u}^{(I)}), \quad (2.17)$$

where $\frac{D_0}{Dt}$ is the convective derivative associated with the mean flow, and c_0 and ρ_0 are, respectively, the mean flow speed of sound and density. ϕ is related to the pressure by

$$p' = -\rho_0(\vec{x})\frac{D_0\phi}{Dt}. \qquad (2.18)$$

The vortical component $\vec{u}^{(I)}$ is in general not solenoidal, but it does become solenoidal far upstream where the mean flow is uniform. For flows with no upstream entropy disturbances, $\vec{u}^{(I)}$ is given by

$$u_i^{(I)} = \vec{u}_\infty(\vec{X} - \vec{i}U_\infty t)\cdot\frac{\partial\vec{X}}{\partial x_i}. \qquad (2.19)$$

The components of $(\vec{X} - \vec{i}U_\infty t)$, where $\vec{X} = (X_1, X_2, X_3)$, are essentially Lagrangian coordinates of the mean flow fluid particles. $X_2 = X_2(x_1, x_2, x_3)$ and $X_3 = X_3(x_1, x_2, x_3)$ are functionally independent integrals of the equations

$$\frac{dx_1}{U_1} = \frac{dx_2}{U_2} = \frac{dx_3}{U_3} \qquad (2.20a)$$

such that

$$X_2 \rightarrow x_2 \quad \text{and} \quad X_3 \rightarrow x_3 \quad \text{as} \quad x_1 \rightarrow -\infty. \qquad (2.20b)$$

For two-dimensional mean flow, we may take

$$X_2 = \frac{\Psi_0}{\rho_\infty U_\infty} \qquad (2.21)$$

and

$$X_3 = x_3, \qquad (2.22)$$

where Ψ_0 is the stream function of the mean flow and x_3 is the spatial coordinate in the spanwise direction. The component X_1 is defined by

$$X_1 = U_\infty\Delta, \qquad (2.23)$$

where Δ is the Lighthill "Drift" function [12], which can be expressed in terms of Φ_0 and Ψ_0 as

$$\Delta = \frac{\Phi_0}{U_\infty^2} + \int_{-\infty}^{\Phi_0}\left(\frac{1}{U_0^2} - \frac{1}{U_\infty^2}\right)d\Phi_0, \qquad (2.24)$$

where the integration is carried out on $\Psi_0 = $ constant. The difference in Δ between two points on a streamline is the time it takes a mean flow fluid particle to traverse the distance between those two points.

To complete the formulation of the problem, it is necessary to specify boundary conditions for the unsteady potential ϕ. At the surface of the airfoil, the normal velocity component must vanish, so that ϕ must satisfy

$$(\vec{u}^{(I)} + \vec{\nabla}\phi)\cdot\vec{n} = 0 \qquad (2.25)$$

or

$$\frac{\partial\phi}{\partial n} = -\vec{u}^{(I)}\cdot\vec{n}, \qquad (2.26)$$

where $\vec{n}$ is the unit normal at the surface of the airfoil. In the wake, the pressure is continous so that ϕ must obey

$$\frac{D_0}{Dt}(\triangle\phi) = 0, \qquad (2.27)$$

where $\triangle\phi$ is the jump in ϕ across the vortex sheet behind the airfoil. Far upstream, ϕ must satisfy

$$\phi \rightarrow 0 \quad \text{as} \quad x_1 \rightarrow -\infty. \qquad (2.28)$$

Atassi and Grzedzinski's Decomposition of the Unsteady Velocity

For most flows of practical aerodynamic interest, there will be a stagnation point near the leading edge of the airfoil where the mean velocity U_0 vanishes. At this point the Drift function Δ has a logarithmic singularity, and the right hand side of (2.19) then has a nonintegrable reciprocal singularity. Since Δ is additive, the right hand side of (2.19) will remain undefined along the surface of the airfoil and in its wake. Equation (2.26) then shows that the boundary condition for ϕ is singular along the airfoil surface. Because of these difficulties we conclude that it is not possible to use Goldstein's approach directly for numerical computations of unsteady vortical flows around aerodynamic bodies with a stagnation point.

Atassi and Grzedzinski [5] have shown that it is possible to modify Goldstein's splitting of the unsteady velocity field in such a way as to remove the singular and indeterminate character of the resulting boundary condition for the unsteady potential at the airfoil surface. In their decomposition of the unsteady velocity, $\vec{u}$ is split into the sum of a known vortical component $\vec{u}^{(R)}$, which has zero normal and streamwise velocity components on the airfoil and in the wake, and an unkown potential component ϕ^* that satisfies equation (2.17) with a modified source term, so that

$$\vec{u}(\vec{x}, t) = \vec{u}^{(R)} + \vec{\nabla}\phi^* \qquad (2.29)$$

where ϕ^* satisfies

$$\frac{D_0}{Dt}\left(\frac{1}{c_0{}^2}\frac{D_0\phi^*}{Dt}\right) - \frac{1}{\rho_0}\vec{\nabla}\cdot(\rho_0\vec{\nabla}\phi^*) = \frac{1}{\rho_0}\vec{\nabla}\cdot(\rho_0\vec{u}^{(R)}) \quad (2.30)$$

The vortical component $\vec{u}^{(R)}$ is given by

$$\vec{u}^{(R)} = \vec{u}^{(I)} + \vec{\nabla}\tilde{\phi}, \qquad (2.31)$$

where $\tilde{\phi}$ is a function that satisfies

$$\frac{D_0\tilde{\phi}}{Dt} = 0. \qquad (2.32)$$

As is shown in [5], there is no pressure associated with the velocity $\vec{\nabla}\tilde{\phi}$, so that the vortical velocity $\vec{u}^{(R)}$ produces no pressure fluctuations. The pressure is determined entirely by ϕ^* and is given by

$$p' = -\rho_0(\vec{x})\frac{D_0\phi^*}{Dt}. \qquad (2.33)$$

In order to choose a particular function $\tilde{\phi}$ that cancels the singular behavior of $\vec{u}^{(I)}$ along the surface of the airfoil and in its wake, the boundary condition

$$(\vec{u}^{(I)} + \vec{\nabla}\tilde{\phi})\cdot\vec{n} = 0 \qquad (2.34)$$

is imposed at the airfoil surface and in the wake. Condition (2.34) should be understood as the limit as we move close to the airfoil and the wake. Details concerning the construction of the function ϕ can be found in [5]. For the important special case of incident harmonic velocity disturbances, specific formulas for $\tilde{\phi}$ are presented in [5], and will be discussed shortly in the present paper.

The function $\vec{u}^{(R)}$ has zero normal and streamwise velocity components at the airfoil surface and in the wake, so that $\vec{u}^{(R)}$ satisfies

$$\vec{u}^{(R)}\cdot\vec{n} = 0, \qquad (2.35)$$

and

$$\vec{u}^{(R)}\cdot\vec{\tau} = 0, \qquad (2.36)$$

where $\vec{n}$ and $\vec{\tau}$ are the unit normal and tangent vectors. The airfoil boundary condition for ϕ^* is then

$$(\vec{u}^{(R)} + \vec{\nabla}\phi^*)\cdot\vec{n} = 0 \qquad (2.37)$$

which reduces to simply

$$\vec{\nabla}\phi^*\cdot\vec{n} = 0. \qquad (2.38)$$

In addition to satisfying the governing equation (2.30) and the airfoil boundary condition (2.38), the unsteady potential ϕ^* must also satisfy appropriate boundary conditions in the far field, in the wake, and at the airfoil trailing edge.

In the far field, equations (2.29) and (2.31) together with condition (2.13) imply that ϕ^* must satisfy

$$\vec{\nabla}\phi^* \to -\vec{\nabla}\tilde{\phi} \quad \text{as} \quad x_1 \to -\infty. \qquad (2.39)$$

In the wake of the airfoil, ϕ^* is not continuous but must satisfy a jump condition determined by the continuity of the unsteady pressure. Applying (2.33) on each side of the vortex sheet behind the airfoil leads to the condition

$$\frac{D_0}{Dt}(\triangle\phi^*) = 0 \qquad \text{wake} \qquad (2.40)$$

Finally, at the trailing edge point ϕ^* must be continuous in the streamwise direction to ensure satisfaction of the Kutta condition.

Upstream Disturbances

In a previous paper [13] the authors have shown that the most general upstream vortical disturbances can be represented as the sum of three-dimensional, harmonic vorticity waves in the airfoil frame of reference. Because the governing equation (2.30) is linear, we can without loss of generality consider a single Fourier component of the incident disturbance, and obtain the solution to more general disturbances by superposition. We therefore consider incident velocity disturbances of the form

$$\vec{u}_\infty = \vec{a}e^{i\vec{k}\cdot(\vec{x}-\vec{i}U_\infty t)} \qquad (2.41)$$

where $|\vec{a}| \ll U_\infty$, $\vec{k}$ is the wave number vector which specifies the direction of propagation of the gust, and $\vec{a}$ and $\vec{k}$ must satisfy

$$\vec{a}\cdot\vec{k} = 0 \qquad (2.42)$$

in order to ensure that $\vec{u}_\infty$ is solenoidal (satisfies the continuity equation).

Now condition (2.13) shows that the unsteady velocity $\vec{u}(\vec{x}, t)$ must satisfy

$$\vec{u}(\vec{x}, t) \to \vec{a}e^{i\vec{k}\cdot(\vec{x}-\vec{i}U_\infty t)} \qquad \text{as} \qquad x_1 \to -\infty. \quad (2.43)$$

Since $X_2 = \frac{\Psi_0}{\rho_\infty U_\infty}$ and Ψ_0 is the stream function of a two-dimensional mean flow,

$$X_2 \to x_2 + \frac{\Gamma}{2\pi U_\infty}\ln(x_1{}^2 + x_2{}^2) + \text{constant as } x_1 \to -\infty, \qquad (2.44)$$

so that we do not have $X_2 \to x_2$ at upstream infinity, as required by condition (2.20b). Equations (2.29), (2.31), and (2.39) together with (2.19) then show that

$$\vec{u}(\vec{x}, t) \to \vec{a}e^{i\vec{k}\cdot(x_1-U_\infty t, x_2+\frac{\Gamma}{2\pi U_\infty}\ln(x_1{}^2+x_2{}^2)+\text{constant}, x_3)}$$

$$\text{as} \qquad x_1 \to -\infty, \qquad (2.45)$$

so that (2.43) is not satisfied.

However, as discussed by Atassi [3], for a real airfoil of finite span, $X_2 \to x_2 + \text{constant}$. The two-dimensional approximation is only valid then for distances that are small compared to the airfoil span, but large compared to the chord. Thus, (2.44) should be considered in this limit.

5

In order to avoid difficulties with upstream conditions, the imposed upstream disturbances should then take the general form

$$\vec{u}_\infty = \vec{a}e^{i\vec{k}\cdot(\vec{X}-\vec{i}U_\infty t)} \qquad (2.46)$$

where $\vec{X}$ is defined by (2.21) - (2.23). Then with this definition of $\vec{u}_\infty$, equations (2.19) and (2.45) show that condition (2.13) will be satisfied.

The Boundary Value Problem

We now summarize the boundary value problem that has been developed. For convenience, we drop the $\star$ notation which was used to distinguish between the formulation of Atassi and Grzedzinski and the formulation of Goldstein.

We consider a potential mean flow about a two-dimensional airfoil of infinite span with three-dimensional, rotational velocity disturbances of the form

$$\vec{u}_\infty = \vec{a}e^{i\vec{k}\cdot(\vec{X}-\vec{i}U_\infty t)} \qquad (2.47)$$

imposed upstream (See Figure 1). The amplitude $\vec{a}$ satisfies $|\vec{a}| \ll U_\infty$, and $\vec{X}$ is defined by equations (2.21) through (2.23).
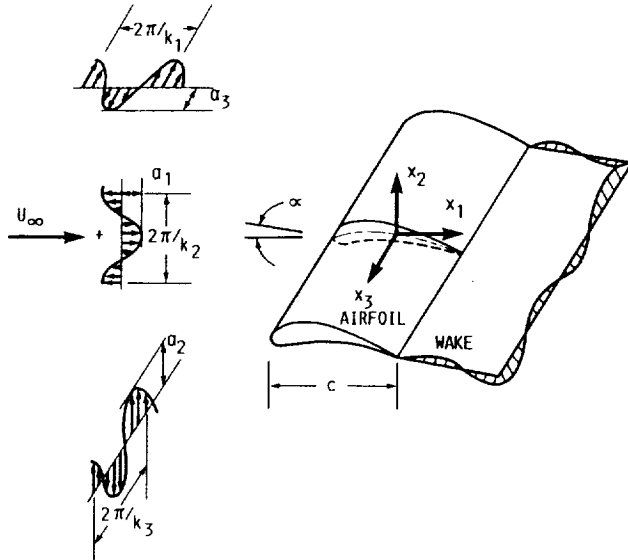
FIGURE 1. - AIRFOIL IN A THREE-DIMENSIONAL GUST.

The unsteady potential obeys the convective wave equation

$$\frac{D_0}{Dt}\left(\frac{1}{c_0{}^2}\frac{D_0\phi}{Dt}\right) - \frac{1}{\rho_0}\vec{\nabla}\cdot(\rho_0\vec{\nabla}\phi) = \frac{1}{\rho_0}\vec{\nabla}\cdot(\rho_0\vec{u}^{(R)}), \quad (2.48)$$

where the unsteady velocity is given by

$$\vec{u}(\vec{x},t) = \vec{u}^{(R)} + \vec{\nabla}\phi \qquad (2.49)$$

and the unsteady pressure is determined from

$$p' = -\rho_0(\vec{x})\frac{D_0\phi}{Dt}. \qquad (2.50)$$

In addition, ϕ must satisfy the boundary conditions

$$\vec{\nabla}\phi\cdot\vec{n} = 0 \qquad \text{airfoil surface} \qquad (2.51)$$

$$\frac{D_0}{Dt}(\triangle\phi) = 0 \qquad \text{wake} \qquad (2.52a)$$

$$\triangle[\vec{\nabla}\phi\cdot\vec{n}] = 0 \qquad \text{wake} \qquad (2.52b)$$

$$\vec{\nabla}\phi \rightarrow -\vec{\nabla}\tilde{\phi} \quad \text{as} \quad x_1 \rightarrow -\infty, \qquad (2.53)$$

and be continuous in the streamwise direction at the airfoil trailing edge. Note that for completeness we have also included boundary condition (2.52b), which imposes continuity of the normal velocity across the wake. For nonlifting airfoils this condition is automatically satisfied, since in that case ϕ is an odd function with respect to X_2. For lifting airfoils, however, ϕ is no longer an odd function and condition (2.52b) must be imposed.

To complete the mathematical formulation of the boundary value problem, the explicit expression of the function $\tilde{\phi}$ must be given. For a complete discussion of the derivation of $\tilde{\phi}$ for the general problem of arbitrary upstream disturbances, the reader should consult Reference 5. For the problem of periodic disturbances of the form (2.47) imposed upstream of a single obstacle which is two-dimensional (such as an isolated airfoil), it is shown in [5] that $\tilde{\phi}$ is given by

$$\tilde{\phi} = \frac{i}{k_1}\left(a_1 + \frac{a_2 k_1 - a_1 k_2}{1 + i a_0 U_\infty k_1}\frac{1 - e^{-ik_2 X_2}}{k_2}\right)e^{i\vec{k}\cdot(\vec{X}-\vec{i}U_\infty t)}, \qquad (2.54)$$

where

$$\vec{a} = (a_1, a_2, a_3) \quad \text{and} \quad a_0 = -\left(\frac{\partial U_0}{\partial n}\right)_S^{-1} \qquad (2.55)$$

and n denotes the direction of the outward unit normal, S denotes the stagnation point near the airfoil leading edge, and $U_0 = |\vec{U}_0|$ is the magnitude of the mean velocity.

With this definition of $\tilde{\phi}$, and with the upstream velocity disturbances given by (2.47), the vortical velocity may then be written

$$\vec{u}^{(R)} = [\vec{\nabla}(\vec{a}\cdot\vec{X})]e^{i\vec{k}\cdot(\vec{X}-\vec{i}U_\infty t)} + \vec{\nabla}\tilde{\phi}. \qquad (2.56)$$

This completes the linearized mathematical formulation of the general boundary value problem for the case of unsteady vortical flow past a lifting airfoil.

III. Basic Numerical Approach

Reformulation and Nondimensionalization of the Boundary Value Problem

For numerical purposes it is necessary to reformulate the boundary value problem presented in the previous section into a form more suitable for numerical computations. Of particular concern is condition (2.53). In order to facilitate the implementation of the far field boundary condition, it is convenient to replace ϕ by a function whose gradient vanishes as $r \rightarrow \infty$, where r is the distance from the airfoil center.

To this end, we introduce the potential functions ϕ_1 and ϕ_2, where

$$\phi = \phi_1 - \phi_2 \qquad (3.1)$$

and ϕ_2 is a known function which is constructed such that

$$|\phi_2 - \tilde{\phi}| \to 0 \quad \text{as} \quad r \to \infty. \qquad (3.2)$$

Equation (3.1) together with conditions (2.53) and (3.2) then show that the new potential function ϕ_1 will satisfy

$$\vec{\nabla}\phi_1 \to \vec{\nabla}\phi_2 - \vec{\nabla}\tilde{\phi} \to 0 \quad \text{as} \quad r \to \infty. \qquad (3.3)$$

The problem may then be reformulated in terms of the unknown potential ϕ_1.

In the present paper we will not concern ourselves with the explicit expression of the potential function ϕ_2. The reader may consult [8] or [9] for details.

Before presenting the reformulated boundary value problem in terms of the potential ϕ_1, we present the nondimensionalization of the problem. We normalize as follows:

	by	
$x_1, x_2, x_3, X_1, X_2, X_3$	by	$\frac{c}{2}$
Φ_0	by	$\frac{c}{2}U_\infty$
Ψ_0	by	$\frac{c}{2}\rho_\infty U_\infty$
U_0, c_0	by	U_∞
ρ_0	by	ρ_∞
p'	by	$\rho_\infty U_\infty |\vec{a}|$
t, Δ	by	$\frac{c}{2U_\infty}$
ω	by	$\frac{2U_\infty}{c}$
k_1, k_2, k_3	by	$\frac{2}{c}$
$\phi, \tilde{\phi}, \phi_1, \phi_2$	by	$\frac{c}{2}|\vec{a}|$
$\vec{a}$	by	$|\vec{a}|$

The normalized wave number $k_1 = \frac{\omega c}{2U_\infty}$, where ω and U_∞ are the dimensional angular frequency and free stream velocity, respectively, is called the reduced frequency.

We will assume throughout the remainder of the present section that all quantities are nondimensional.

The governing equation for ϕ_1 is then

$$\frac{D_0}{Dt}\left(\frac{1}{c_0{}^2}\frac{D_0\phi_1}{Dt}\right) - \frac{1}{\rho_0}\vec{\nabla}\cdot(\rho_0\vec{\nabla}\phi_1) = \qquad (3.4)$$

$$\frac{1}{\rho_0}\vec{\nabla}\cdot(\rho_0\vec{u}^{(R)}) + \frac{D_0}{Dt}\left(\frac{1}{c_0{}^2}\frac{D_0\phi_2}{Dt}\right) - \frac{1}{\rho_0}\vec{\nabla}\cdot(\rho_0\vec{\nabla}\phi_2)$$

and the boundary conditions are

$$\vec{\nabla}\phi_1 \cdot \vec{n} = \vec{\nabla}\phi_2 \cdot \vec{n} \qquad \text{airfoil surface} \qquad (3.5)$$

$$\frac{D_0}{Dt}[\Delta(\phi_1 - \phi_2)] = 0 \qquad \text{wake} \qquad (3.6a)$$

$$\Delta[\vec{\nabla}(\phi_1 - \phi_2)\cdot\vec{n}] = 0 \qquad \text{wake} \qquad (3.6b)$$

$$\vec{\nabla}\phi_1 \to 0 \quad \text{as} \quad x_1 \to -\infty. \qquad (3.7)$$

Finally, the nondimensional expressions for the potential function $\tilde{\phi}$, for the unsteady velocity, the vortical velocity, and for the upstream velocity disturbances are

$$\tilde{\phi} = \frac{i}{k_1}\left(a_1 + \frac{a_2k_1 - a_1k_2}{1 + ia_0k_1}\frac{1 - e^{-ik_2X_2}}{k_2}\right)e^{i\vec{k}\cdot\vec{X} - ik_1 t} \qquad (3.8)$$

where

$$X_1 = \Delta, \quad X_2 = \Psi_0, \quad X_3 = x_3 \qquad (3.9)$$

$$\vec{u}(\vec{x}, t) = \vec{u}^{(R)} + \vec{\nabla}(\phi_1 - \phi_2) \qquad (3.10)$$

where

$$\vec{u}^{(R)} = [\vec{\nabla}(\vec{a}\cdot\vec{X})]e^{i\vec{k}\cdot\vec{X} - ik_1 t} + \vec{\nabla}\tilde{\phi}. \qquad (3.11)$$

$$\vec{u}_\infty = \vec{a}e^{i\vec{k}\cdot\vec{X} - ik_1 t} \qquad (3.12)$$

Determination of Mean Potential Flow

In order to obtain numerical solutions to equation (3.4) and its associated boundary conditions, one must first obtain the steady potential flow about the airfoil for the given flow conditions. This will in general require the use of a standard potential flow solver such as FLO36.[14]

However, an examination of equations (3.8) through (3.12) indicate that the most natural choice of independent variables in which to solve equation (3.4) are Φ_0 and Ψ_0, the mean flow potential and stream functions. Since standard potential flow codes solve the steady problem in terms of the spatial coordinates x_1 and x_2, there is some difficulty in obtaining the steady solution as a function of Φ_0 and Ψ_0.

Another difficulty arises due to the fact that the grids used by steady flow solvers are not suitable for the unsteady calculation. As reported in References 13 and 15, accurate solution of equation (3.4) over a large range of flow conditions requires using grids which are determined as a function of both the reduced frequency k_1 and the free stream Mach number M_∞. This means that in general it will be necessary to interpolate the solution from the steady grid onto the appropriate unsteady grid.

Because of the loss of accuracy that can result from such an interpolation process, and also because of the need to know the mean flow as a function of Φ_0 and Ψ_0, an analytical scheme that can obtain the compressible, subsonic flow about isolated airfoils was developed. The scheme is based on the idea that, except for a small inner region surrounding the airfoil, the flow gradients are not too large. Thus in the large outer region extending to infinity, the mean flow is essentially governed by a set of linear equations. As a result, one can use Gothert's Rule, whereby the compressible flow about a given airfoil can be obtained from the incompressible flow about a similar airfoil.

The only limitation in obtaining the mean potential flow by this particular approach is that the method will not give a good approximation in the inner region and particularly near the stagnation point. However, extensive testing of this approach and comparing with the steady potential

flow solver FLO36 has shown that the region of inaccuracy is very small. Results that are presented in [8], but which are not reproduced here due to a lack of space, show that the agreement overall is quite good, with the exception of grid points on the airfoil surface that are near the stagnation point. Because of this inaccuracy, we use FLO36 to calculate the mean flow quantities along the airfoil surface itself, and use the approximate analytical scheme off the airfoil except in a small region just upstream of the stagnation point. In this region, for airfoils that have steady loading, the velocities are calculated using a Taylor series expansion. For airfoils without steady loading, the velocities are calculated from a local analytical solution which is patched to the outer solution.

For complete details concerning this method of determining the mean flow, the reader should consult [8].

Frequency Domain Formulation

An inspection of equations (3.8), (3.11), and (3.12) indicates that the time dependence of the present boundary value problem comes entirely through the harmonic term e^{-ik_1t}. It is therefore possible to make a transformation from the time domain into the frequency domain by a simple change of dependent variable. By transforming the problem into the frequency domain, time is completely eliminated from the problem and it is possible to significantly simplify the mathematical formulation of the boundary value problem.

For the case of two-dimensional mean flow, we transform into the frequency domain by making the following change of dependent variable:

$$\phi_1 = \varphi e^{-ik_1t + ik_3x_3} \qquad (3.13)$$

By including the ik_3x_3 term in the transformation, the harmonic dependence on the spanwise component x_3 is also eliminated, since all of the $e^{ik_3x_3}$ terms then factor out from each side of the equation. This is of course possible in view of (3.9) and (3.12).

In addition to the frequency domain transformation (3.13), we also introduce the following change of both dependent and independent variables:

$$\varphi = \psi e^{-iK_0\Phi} \quad \text{where} \quad K_0 = \frac{k_1 M_\infty^2}{\beta_\infty^2} \qquad (3.14)$$

and

$$\Phi = \Phi_0 \qquad (3.15a)$$
$$\Psi = \beta_\infty \Psi_0 \qquad (3.15b)$$

where $\beta_\infty = \sqrt{1 - M_\infty^2}$, and M_∞ is the free stream Mach number.

By making this coordinate transformation, equation (3.4) will reduce to a Helmholtz equation in the far field. This is particularly advantageous for the implementation of the far field boundary condition.

The frequency domain governing equation then takes the following form:

$$-\beta_\infty^2 \left[\frac{\partial^2 \psi}{\partial \Phi^2} + \frac{\partial^2 \psi}{\partial \Psi^2} + \left(\frac{k_1^2 M_\infty^2}{\beta_\infty^4} - \frac{k_3^2}{\beta_\infty^2} \right) \psi \right]$$

$$+ A_1 \psi + A_2 \frac{\partial \psi}{\partial \Phi} + A_3 \frac{\partial \psi}{\partial \Psi} + A_4 \frac{\partial^2 \psi}{\partial \Phi^2} + A_5 \frac{\partial^2 \psi}{\partial \Psi^2}$$

$$= e^{iK_0\Phi}(S_1 + S_2 + S_3 - S_4) \qquad (3.16)$$

where the coefficients $A_1...A_5$ are known functions which depend on the mean flow, and $S_1...S_4$ are given by

$$e^{-ik_1t + ik_3x_3} S_1 = \frac{\vec{\nabla}\rho_0}{\rho_0} \cdot \{[\vec{\nabla}(\vec{a} \cdot \vec{X})]e^{i\vec{k}\cdot\vec{X} - ik_1t} + \vec{\nabla}\tilde{\phi}\} \qquad (3.17a)$$

$$e^{-ik_1t + ik_3x_3} S_2 = \vec{\nabla} \cdot \{[\vec{\nabla}(\vec{a} \cdot \vec{X})]e^{i\vec{k}\cdot\vec{X} - ik_1t} + \vec{\nabla}\tilde{\phi}\} \qquad (3.17b)$$

$$e^{-ik_1t + ik_3x_3} S_3 = \frac{D_0}{Dt}\left(\frac{1}{c_0^2}\frac{D_0\phi_2}{Dt}\right) \qquad (3.17c)$$

$$e^{-ik_1t + ik_3x_3} S_4 = \frac{1}{\rho_0}\vec{\nabla} \cdot (\rho_0\vec{\nabla}\phi_2) \qquad (3.17d)$$

In the far field both the coefficients $A_1...A_5$ and the source term $S_1 + S_2 + S_3 - S_4$ tend to zero.

Our basic numerical approach to solving equation (3.16) is to use the method of finite difference approximations. By discretizing the flow field and employing finite differences at each grid point, a large linear system of equations is obtained which can be solved using a matrix solver.

Previous experience in solving equation (3.16) for the case of flat plate and symmetric airfoils has shown that the independent variables (Φ, Ψ) are not suitable computational coordinates for the gust response problem [13,15]. There are difficulties in obtaining consistently accurate results over a large range of Mach numbers and reduced frequencies, and also problems with the implementation of far field boundary conditions. A transformation of the independent variables is needed which not only provides an adequate distribution of grid points around the airfoil in the near field, but also provides a distribution of grid points in the far field which is suitable for acoustic wave propagation and the implementation of far field, radiation type boundary conditions.

In order to satisfy these requirements, we make a transformation into the elliptic coordinates (η, ξ) with the transformation

$$\Phi = a^* \cos(\pi\eta)\cosh(\pi\xi) \qquad (3.18a)$$

$$\Psi = a^* \sin(\pi\eta)\sinh(\pi\xi) \qquad (3.18b)$$

where a^* is an arbitrary constant (See [8] for the definition of a^*). Note that in the far field the elliptic coordinates reduce essentially to cylindrical coordinates, and that the

$\Phi - \Psi$ plane is mapped into a semi-infinite strip in the $\eta - \xi$ plane.

With this change of variables, the governing equation takes the form

$$-\beta_\infty^2 \left[\frac{\partial^2 \psi}{\partial \eta^2} + \frac{\partial^2 \psi}{\partial \xi^2} + J(\eta, \xi)\left(\frac{k_1^2 M_\infty^2}{\beta_\infty^4} - \frac{k_3^2}{\beta_\infty^2}\right)\psi\right]$$

$$+ A_1 J(\eta, \xi)\psi + T_1 \frac{\partial \psi}{\partial \xi} + T_2 \frac{\partial \psi}{\partial \eta}$$

$$+ T_3 \frac{\partial^2 \psi}{\partial \xi^2} + T_4 \frac{\partial^2 \psi}{\partial \eta^2} + T_5 \frac{\partial^2 \psi}{\partial \eta \partial \xi}$$

$$= e^{iK_0 \Phi}(S_1 + S_2 + S_3 - S_4) J(\eta, \xi), \qquad (3.19)$$

where $J(\eta, \xi)$ is the Jacobian of the transformation (3.18), and $T_1...T_5$ are known functions of (η, ξ) which depend upon the mean flow.

The frequency domain boundary value problem then consists of the governing equation (3.19) and boundary conditions (3.5) - (3.7), together with the requirement that the velocity is finite at the trailing edge.

However, we point out that condition (3.7), which requires that $\vec{\nabla}\phi_1 \rightarrow 0$ at upstream infinity, cannot be imposed throughout the far field on a boundary at a finite distance from the airfoil. To implement such a condition would impose a reflecting boundary condition which can lead to large errors in the solution.

To correctly model the physics of the present unsteady boundary value problem requires that the far field boundary condition be such that it allows outgoing acoustic waves to leave the solution domain without being reflected back into the computational grid. While this can be done in more than one way, the authors have found that the best approach is to use a Sommerfield radiation condition on the unsteady pressure. This approach is easy to implement and has the advantage of giving an accurate far field solution from which the acoustic radiation can be calculated.

Our far field boundary condition is then given by

$$\left[\frac{\partial}{\partial R} - i\sqrt{\left(\frac{k_1 M_\infty}{\beta_\infty^2}\right)^2 - \left(\frac{k_3}{\beta_\infty}\right)^2}\right]\left(\frac{\partial}{\partial \Phi} - i\frac{k_1}{\beta_\infty^2}\right)\psi = 0 \quad (3.20)$$

where

$$\Phi = R \cos \Theta \qquad (3.21a)$$
$$\Psi = R \sin \Theta. \qquad (3.21b)$$

This condition is applied for all grid points on the far field boundary.

Numerical Solution Procedure

The problem to be solved numerically consists of the governing equation (3.19) and the boundary conditions (3.5), (3.6a), (3.6b), and (3.20). As our major purpose in the present paper is to present the formulation of the boundary value problem and to discuss numerical results, we will not discuss the remaining details of our numerical approach. The interested reader should consult [8] or [9]. We do, however, present the following general information about our numerical solution procedure.

First, our basic numerical approach is to use the method of finite difference approximations and to solve the resulting matrix equation using a direct, sparse matrix solver. The governing equation is modelled using nine-point central differencing, and the airfoil and far field boundary conditions are satisfied using four-point, one-sided differencing. The wake boundary condition (3.6b) is satisfied using three-point, one-sided differencing both above and below the wake.

Second, we point out that it is essential that the source term be evaluated accurately in order to obtain accurate solutions to the problem. This depends largely upon an accurate evluation of the Drift function defined by equation (2.24), and upon an accurate evaluation of the potential functions ϕ_2 and $\tilde{\phi}$ so that condition (3.2) is satisfied in the numerical implementation.

Finally, we mention that obtaining accurate solutions to the present wave propagation problem requires using grids which are determined as a function of both the Mach number and reduced frequency [13,15]. See [8] or [9] for details on how this is done for the lifting airfoil problem.

IV. Discussion of Numerical Results

Our major purpose in the presentation and discussion of numerical results is to demonstrate the effects of airfoil thickness, angle of attack, camber, and Mach number on the airfoil unsteady response to imposed upstream rotational velocity disturbances (gusts). We will examine in detail the effects of each of these parameters on the unsteady lift and moment of airfoils subjected to one-, two-, and three-dimensional gusts.

The authors would like to emphasize that great care was taken to validate the codes that were used to obtain the numerical results presented in this section. Due to a lack of space, however, we will not concern ourselves with the validation process in the present work. Information concerning the steps that were taken to validate our numerical scheme can be found in References 8, 9, and 15.

Before discussing the unsteady results, we show plots of the mean flow Mach number at the airfoil surface for the various flow configurations that were considered in the present work. These plots are shown in Figures 2 through 9. All of the airfoils used for these calculations were Joukowski airfoils of various geometries. The Mach number results shown in these figures, with the exception of the incompressible results in Figure 8, were obtained from the steady potential flow solver FLO36.[14] The incompressible results were obtained from the known analytical solution for the ideal flow around a Joukowski airfoil.

Figures 2 and 3 present results for a 12% thick symmetric airfoil at zero degrees incidence for Mach numbers of .5 and .7, respectively. Even though these airfoils are unloaded, their thickness alters the mean flow considerably from the linear thin airfoil case where the Mach number is constant throughout the flow. Note that for the higher Mach number case the mean flow variation is much stronger. It will be seen shortly that even this amount of mean flow variation can have a significant effect on the unsteady flow due to the distortion of the vortical structure of the upstream disturbances.

Figures 4 - 9 present results for airfoils with steady loading. The results in Figure 4 are for a 12% thick symmetric airfoil at an angle of attack of 5°, and the results in Figure 5 are for a 12% thick airfoil with 5% camber but 0° angle of attack. The free stream Mach number for both of these plots is .5. Note that for the uncambered airfoil with 5° angle of attack, the loading is concentrated near the leading edge, whereas for the cambered airfoil with zero incidence angle the loading is distributed more evenly over the entire airfoil. Note also that even though the gradients in the flow for Figure 4 are much stronger than for the results in Figure 5, the airfoil in Figure 5 has the larger steady lift coefficient. As will be seen later, the magnitude of the steady lift coefficient is in some sense a good measure of the amount of mean flow distortion for lifting airfoils over nonlifting airfoils.

In Figures 6 and 7, we present results for airfoils with 2° angle of attack, 5% camber, and a free stream Mach number of .5. The thickness ratios are .06 and .12, respectively. Because of the larger thickness ratio, the airfoil in Figure 7 has a much smoother Mach number profile near the leading edge, and also a slightly larger steady lift coefficient. Due to its heavier loading, the airfoil in Figure 7 will have a stronger distortion effect on the incident vortical disturbances than will the airfoil in Figure 6, even though their angle of attack and camber ratios are the same.

Finally, in Figures 8 and 9, results are presented for 12% thick symmetric airfoils at 3° angle of attack with free stream Mach numbers of .1 and .6, respectively. Note that, due to compressibility effects, the increase in the Mach number leads to much stronger gradients in the mean flow. Again we would expect the stronger mean flow variation to in turn lead to a stronger distortion of the impinging gusts.

We now turn our attention to the unsteady results presented in Figures 10 through 39. The results that are shown are presented in sets of six plots. In each set, the first three plots present results for the normalized unsteady lift, and the next three plots present results for the normalized unsteady moment. The normalized unsteady lift and moment are usually referred to as the response functions and are defined by

$$ R_L(k_1, k_3, M_\infty) = \frac{L'}{\pi \rho_\infty c U_\infty |\vec{a}| e^{i\omega t}} \quad (4.1) $$

and

$$ R_M(k_1, k_3, M_\infty) = \frac{M'}{\frac{\pi}{2} \rho_\infty c^2 U_\infty |\vec{a}| e^{i\omega t}} \quad (4.2) $$

where L' is the unsteady lift and M' is the unsteady moment about the airfoil center.

In Figures 10 through 21 we present results that demonstrate the effects of airfoil thickness on the unsteady response functions. Figures 10 through 15 are for symmetric unloaded airfoils, and Figures 16 through 21 are for loaded airfoils. Figures 22 through 33 present results that demonstrate the effects of mean airfoil loading on the unsteady response functions. In Figures 22 through 27, the induced loading is due to angle of attack, and in Figures 28 through 33 it is due to airfoil camber. Finally, Figures 34 through 39 present results that demonstrate the effects of Mach number on the unsteady response functions.

In each set of six plots, we present results for one-, two-, and three-dimensional gusts – first for the unsteady lift and then for the unsteady moment. The reduced frequency values used in the calculations were the same for all the figures, and were as follows: k_1 = 0, 0.01, 0.03, 0.06, 0.1, 0.2, 0.3, 0.45, 0.6, 0.8, 1.0, 1.3, 1.6, 2.0, 2.5, 3.0, 3.5, and 4.0. For each response function shown, the point on the real axis and furthest to the right corresponds to the quasi-steady case in which k_1 = 0. The other points along the response function curve correspond in order to the reduced frequency values given above.

The conditions on the gust wave number parameters for the plots shown are as follows: for the one-dimensional case, i.e., a transverse gust, k_2 = 0, k_3 = 0, a_1 = 0, a_2 = 1, a_3 = 0; for the two-dimensional gust, i.e., a transverse and longitudinal gust, k_2 = k_1, k_3 = 0, $a_1 = -a_2$, $|\vec{a}|$ = 1, $a_2 > 0$; and for the three-dimensional case k_2 = k_1, k_3 = .4, $\vec{a} \cdot \vec{k}$ = 0, $|\vec{a}|$ = 1, $a_2 > 0$, and $\frac{a_2}{a_1} = -\frac{7}{4}$.

Effects of Airfoil Thickness on the Unsteady Response Functions

In Figures 10 through 15 we compare unsteady results for a zero thickness airfoil versus those for a 12% thick symmetric Joukowski airfoil (See Figure 3). The free stream Mach number is .7, and both airfoils have zero mean loading. It is clear from the results shown in these figures that airfoil thickness can have a strong effect on the unsteady lift and moment, and that the effect depends on both the reduced frequency and the gust wave number conditions.

For the case of the transverse gust, there is a strong effect on both the unsteady lift and moment for both the low and high reduced frequencies. Figure 10 shows that the unsteady lift for the quasi-steady case ($k_1 \rightarrow 0$) is increased by about 16% for the thick airfoil over the flat plate airfoil, and that the magnitude of the unsteady lift is substantially increased for the low reduced frequencies ranging roughly from 0 up to about .1. For the higher frequencies there is a reduction in the unsteady lift and also a change in the phase, whereas in the mid-frequency range of about .2 up to 2, the effect is mainly a change in the phase. The effects of thickness on the unsteady moment are similar to its effect on the unsteady lift, with the exception that the

effect at the higher frequencies is somewhat stronger. For both the unsteady moment and the unsteady lift, the effect of airfoil thickness in the transverse gust case is in general to significantly increase the magnitude of the response for the low reduced frequencies and decrease it for the high reduced frequencies.

In the case of the transverse and longitudinal gust, the effects of airfoil thickness are somewhat different from the transverse gust case, in that there is little effect on the unsteady lift and moment at the lower frequencies. At the higher frequencies, the effect is mainly a reduction in magnitude and a change in phase, analagous to the results for the transverse gust.

The three-dimensional gust results shown in Figures 12 and 15 indicate that the strongest effect of the airfoil thickness occurs for reduced frequencies in the mid-frequency range, rather than for the low or high frequencies as was the case with the 1-D and 2-D gust results. Note that the quasi-steady moment for this case decreases for the thicker airfoil, rather than increasing as in the transverse gust case (Figure 13).

Figures 16 through 21 compare unsteady results for a 6% thick airfoil versus a 12% thick airfoil. The angle of attack and camber ratios of the airfoils are $2°$ and .05, respectively, and the free stream Mach number is .5 (See Figures 6 and 7). The effects of thickness on the unsteady response functions is not as strong in these figures due to both the lower Mach number and the fact that the comparison is between 6% thick and 12% thick airfoils versus 0% and 12% thick airfoils. There are, however, similarities between these results and those described above. For the transverse gust, the effects are mainly to increase the magnitude of the response at the lower frequencies and decrease it at the higher frequencies. For the transverse and longitudinal gust, there is not much effect at the low reduced frequencies, while at the higher frequencies there is a reduction in magnitude analogous to that of the transverse gust case. The three-dimensional gust results in Figures 18 and 21 show little effect due to the change in airfoil thickness.

We conclude that airfoil thickness can have a large effect on the unsteady lift and moment, and that the effect varies considerably depending on both the reduced frequency and the gust wave number parameters. In addition, the results in Figures 10 - 15 show the inability of linear theory to serve as an adequate approximation for flows with mean flow variation which occurs due to airfoil thickness.

Effects of Mean Loading on the Unsteady Response Functions

In Figures 22 - 33 we present results that demonstrate the effects of mean airfoil loading on the unsteady response functions. In Figures 22 - 27, the induced loading is due to angle of attack alone, while in Figures 28 - 33 the induced loading is due to camber alone. The free stream Mach number is .5, the airfoil thickness ratio is .12, and the steady

lift coefficients corresponding to the two loaded airfoils are .72 and .82, respectively (See Figures 2, 4, and 5).

An analysis of the results indicates that there are remarkable similarities between the results shown in Figures 22-24 and Figures 28-30 which demonstrate the effects of mean loading on the unsteady lift.

It is seen that for the case of a transverse gust (Figures 22 and 28), there is virtually no effect on the unsteady lift due to mean loading. This result is in agreement with the theoretical predictions of Atassi [3] concerning the effect of mean airfoil loading on the unsteady lift of airfoils subjected to a transverse gust in incompressible flow. It is interesting that the theoretical result essentially holds also for compressible flows.

Unlike the results for the simple transverse gust, the results for the transverse and longitudinal gust (Figures 23 and 29) show a strong effect due to mean airfoil loading. In both Figures 23 and 29, the effect at the low frequencies is essentially to shift the curve in the direction of the negative real axis. For the results in Figure 23, the reduction in the quasi-steady lift ($k_1 \to 0, k_2 \to 0$) for the loaded airfoil over the unloaded airfoil is 20%, while for the results in Figure 29, the reduction is 23%.

It is clear from the results in these figures that mean airfoil loading leads to a significant reduction in the unsteady lift for the low reduced frequencies of an airfoil in a transverse and longitudinal gust. It turns out that the amount of the reduction in the quasi-steady lift for the two-dimensional gust case is directly proportional to the steady lift coefficient of the loaded airfoil. That is, if we denote the change in the quasi-steady lift from the unloaded airfoil to the loaded airfoil by $\Delta C'_L$, and the proportionality constant by $-K$, we have approximately $\Delta C'_L = -K\,C_L$, where C_L is the steady lift coefficient of the loaded airfoil and K is a constant. It has been determined from the results presented in [8] that the constant $K = .25$. This result is in agreement with the theoretical results of Atassi [3], from which it can be shown that for airfoils with small angle of attack and camber in an incompressible flow, $\Delta C'_L = -\frac{1}{\pi}\frac{k_2}{|k|}\,C_L = -.23 C_L$. The difference in the theoretical value and the numerical value of the proportionality constant can be accounted for by the fact that the theoretical result does not account for the thickness of the airfoil. It is remarkable that the value of $K = .25$ holds for both lightly loaded airfoils and heavily loaded airfoils, and is also nearly independent of the Mach number.

In looking at the three-dimensional gust results in Figures 24 and 30, it is clear that the mean airfoil loading has a strong effect on the unsteady lift for the low reduced frequencies. As in the case of the transverse and longitudinal gust, the effect of the loading in the 3-D case is to significantly reduce the magnitude of the unsteady lift. Interestingly enough, the reduction in the quasi-steady lift for the 3-D case is also proportional to the steady lift coefficient of the loaded airfoil. In this case the value of the proportionality constant K is .10. The reduction in the value of

the proportionality constant for the 3-D case is probably due to the effect of the spanwise wave number k_3. At the present time, however, it is not known to what extent the value of K depends upon k_3.

Unlike the unsteady lift, the unsteady moment responds differently to mean airfoil loading depending upon whether the loading is induced by angle of attack or camber. The results in Figures 26-27 indicate that for the 2-D and 3-D gust cases, the unsteady moment is sensitive to changes in the angle of attack, particularly at the lower frequencies. For the 2-D case, the quasi-steady moment of the loaded airfoil has been reduced by 17% over that of the unloaded airfoil, and for the 3-D case the reduction is 11%. An analysis of the results in Figures 32-33, however, indicates that there is no corresponding reduction in the quasi-steady moment when the mean loading is induced by airfoil camber, and in fact that the camber of the airfoil has almost no effect on the unsteady moment for any range of reduced frequencies.

We conclude, then, that for the airfoils considered in the present work, an increase in angle of attack of an airfoil in a 2-D or 3-D gust leads to a significant reduction in the unsteady moment for the low reduced frequencies, but an increase in the airfoil camber has virtually no effect on the unsteady moment for any range of reduced frequencies.

This is in contrast to the effects of mean loading on the unsteady lift, where both angle of attack and camber lead to a significant reduction in the magnitude of the unsteady response for the low reduced frequencies of the 2-D and 3-D gust cases. Since the reduction of the quasi-steady lift is proportional to the steady lift coefficient and independent of whether the loading is induced by angle of attack or camber, the steady lift coefficient is in some sense a good measure of the amount of mean flow distortion for lifting airfoils over nonlifting airfoils. In addition, this points out that the amount of error made by a numerical scheme which does not take into account the effects of mean flow distortion increases as the steady loading on the airfoil increases.

Effects of Mach Number on the
Unsteady Response Functions

We conclude our discussion of the numerical results by looking at the effects of Mach number on the unsteady response functions. Figures 34 through 39 show comparisons of the unsteady response functions for a symmetric, 12% thick airfoil with 3° angle of attack at Mach numbers of .1 and .6.

An analysis of the results would seem to indicate that the main effect of an increase in Mach number on the unsteady response functions is to substantially increase the magnitude of the unsteady response for the low reduced frequencies, decrease the magnitude at the high frequencies, and alter the phase for the middle frequencies. The increase in magnitude at the low frequencies is quite strong, particularly for the 1-D and 2-D gust cases. For the transverse gust, the quasi-steady lift for the .6 Mach number

airfoil is 30% larger than for the .1 Mach number airfoil. For the transverse and longitudinal gust, the increase is 21%, while for the 3-D gust the increase is only 6%. The percent increase in the quasi-steady moments for the 1-D, 2-D, and 3-D cases are similar.

Although it is not readily apparent from the results in Figures 34-39, another effect of an increase in airfoil Mach number is to intensify the effect of mean flow distortion for a given airfoil configuration. Due to an increase in the Mach number, the mean flow gradients become stronger, and there will be a correspondingly stronger distortion effect upon the oncoming vortical waves. The airfoil selected for the comparison in Figures 34 - 39 is too lightly loaded for this effect to be apparent. The reader may consult [8] for results which demonstrate this phenomenon.

V. Conclusion

In the present paper the authors have presented a linearized unsteady aerodynamic analysis for unsteady vortical flows around lifting airfoils. The first order analysis that we have presented fully accounts for the distortion effects of the nonuniform mean flow, and the results presented have demonstrated that mean flow distortion can have a very strong effect on the unsteady lift and moment.

We conclude on the basis of the numerical results presented in the previous section that our linearized unsteady aerodynamic analysis can be used to solve a wide variety of unsteady vortical flow problems. The results that were presented demonstrated the effects of airfoil thickness, camber, angle of attack, and Mach number on the unsteady lift and moment of Joukowski airfoils in subsonic vortical flows. It was seen that the effects of these parameters on the unsteady response functions varies considerably, depending on the magnitude of the reduced frequency, the Mach number, and the gust wave number conditions. The results presented have thus demonstrated the importance of having a numerical scheme which can handle three-dimensional vortical flows for a large range of Mach numbers and reduced frequencies.

Finally, the authors are in the process of extending the present linearized analysis to include transonic flows. Details will be presented in a future paper.

References

1. Sears, W. R., "Some Aspects of Non-stationary Airfoil Theory and Its Practical Applications." *J. Aero. Sci.*, Vol. 8, No. 3, 1941, pp. 104-108.

2. Goldstein, M. E. and Atassi, H. M., "A Complete Second-Order Theory for the Unsteady Flow About an Airfoil Due to a Periodic Gust," *J. Fluid Mech.*, Vol. 74, 1976, pp. 741-765.

3. Atassi, H.M., "The Sears Problem for a Lifting Airfoil Revisited - New Results," *J. Fluid Mech.* Vol. 141, 1984, pp. 109-122.

4. Goldstein, M. E., "Unsteady Vortical and Entropic Distortions of Potential Flows Round Arbitrary Obstacles," *J. Fluid Mech.*, Vol. 89, 1978, pp. 433-468.

5. Atassi, H. M. and Grzedzinski, J., "Unsteady Disturbances of Streaming Motions Around Bodies," *J. Fluid Mech.*, Vol. 209, Dec. 1989, pp. 385-403.

6. McCroskey, W.J. and Goorjian, P.M., "Interactions of Airfoils with Gusts and Concentrated Vortices in Unsteady Transonic Flow," AIAA Paper 83-1691, July 1983.

7. McCroskey, W. J., "The Effects of Gusts on the Fluctuating Airloads of Airfoils in Transonic Flow," *Journal of Aircraft*, Vol. 22, No. 3, March 1985, pp. 236-243.

8. Scott, J.R., "Compressible Flows with Periodic Vortical Disturbances Around Lifting Airfoils," Ph. D. dissertation in preparation, University of Notre Dame, Notre Dame, IN, 1990.

9. Scott, J.R. and Atassi, H.M., "A Finite-Difference, Frequency-Domain Numerical Scheme for the Solution of the Linearized Unsteady Euler Equations," *Proceedings of the Lewis CFD Symposium on Aeropropulsion*, April 24-26, 1990.

10. Kovasznay, L.S.G., "Turbulence in Supersonic Flow," *J. Aero. Sci.*, Vol. 20, No. 10, 1953, pp. 657-674.

11. Atassi, H.M., "Unsteady Vortical Disturbances Around Bodies," *Proceedings of the Tenth U. S. National Congress of Applied Mechanics*, J.P. Lamb, ed., ASME, 1986, pp. 475-484.

12. Lighthill, M.J., "Drift" *J. Fluid Mech.*, Vol. 1, 1956, pp. 31-53.

13. Atassi, H. M. and Scott, J. R., "Analysis of Nonuniform Subsonic Flows About a Row of Moving Blades," *Proceedings of the Fourth International Symposium on Unsteady Aerodynamics and Aeroelasticity of Turbomachines and Propellers*, H. E. Gallus and S. Servaty, eds., Institute fur Strahlantriebe und Turbomachine, University of Aachen, Federal Republic of Germany, 1988, pp. 39-67.

14. Jameson, A. and Caughey, D.A., "A Finite Volume Method for Transonic Potential Flow Calculations," *Proceedings of the AIAA 3rd Computational Fluid Dynamics Conference*, Williamsburg, Va., July 1979, pp. 122-146.

15. Scott, J. R. and Atassi, H. M., "Numerical Solution of Periodic Vortical Flows About a Thin Airfoil," AIAA Paper 89-1691, June, 1989.
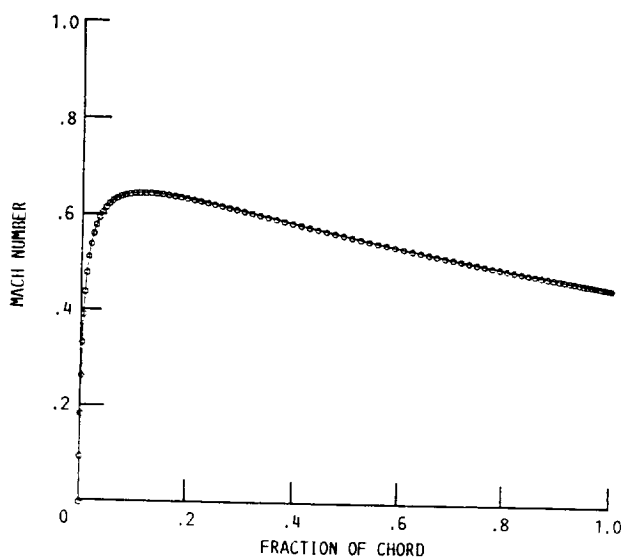
FIGURE 2. - MEAN FLOW MACH NUMBER AT THE AIRFOIL SURFACE FOR A 12 PERCENT THICK JOUKOWSKI AIRFOIL WITH $M_\infty = 5$, $\alpha = 0^0$, AND CAMBER RATIO = 0.0. STEADY $C_L = 0.0$. CALCULATION BY FLO36.
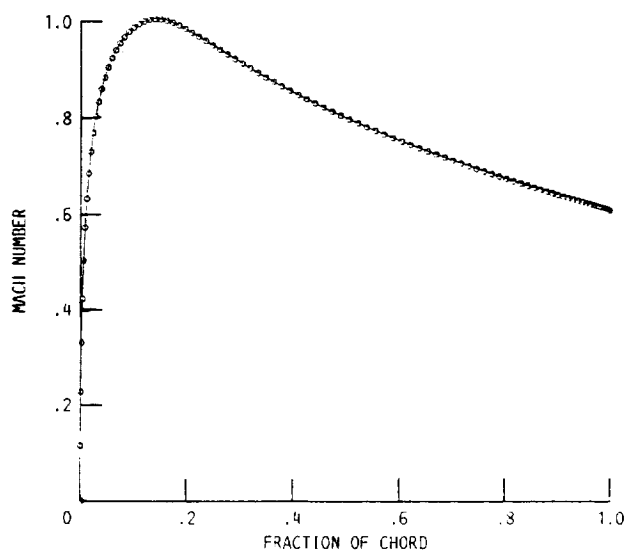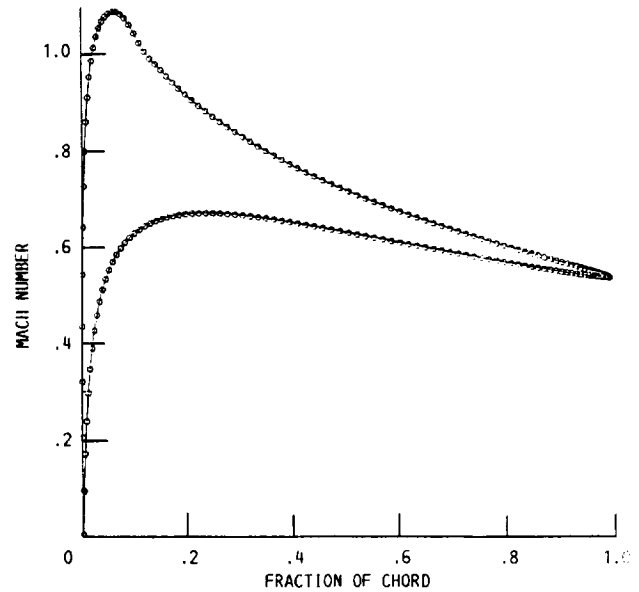

FIGURE 3. - MEAN FLOW MACH NUMBER AT THE AIRFOIL SURFACE FOR A 12 PERCENT THICK JOUKOWSKI AIRFOIL WITH $M_\infty = .7$, $\alpha = 0^0$, AND CAMBER RATIO = 0.0. STEADY $C_L = 0.0$. CALCULATION BY FLO36.
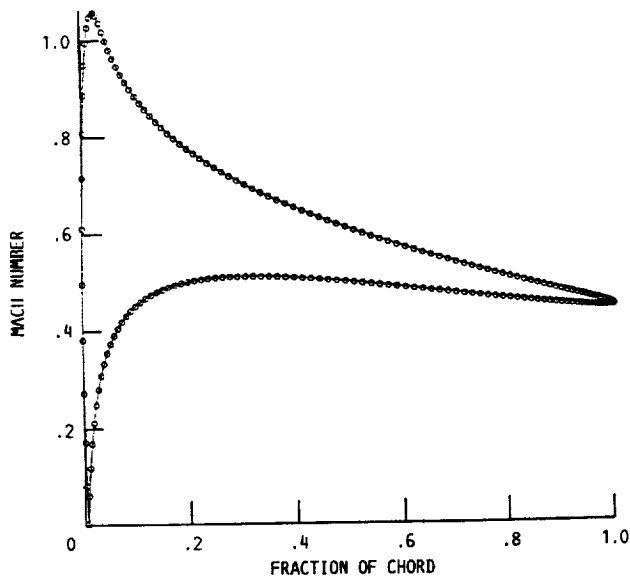
FIGURE 4. - MEAN FLOW MACH NUMBER AT THE AIRFOIL SURFACE FOR A 12 PERCENT THICK JOUKOWSKI AIRFOIL WITH M_∞ = .5, α = 5°, AND CAMBER RATIO = 0.0. STEADY C_L = 0.72. CALCULATION BY FLO36.
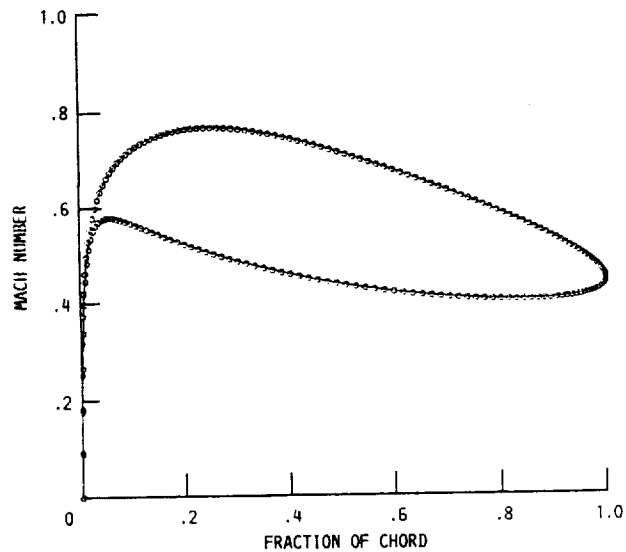
FIGURE 5. - MEAN FLOW MACH NUMBER AT THE AIRFOIL SURFACE FOR A 12 PERCENT THICK JOUKOWSKI AIRFOIL WITH M_∞ = .5, α = 0°, AND CAMBER RATIO = 0.05. STEADY C_L = 0.82. CALCULATION BY FLO36.
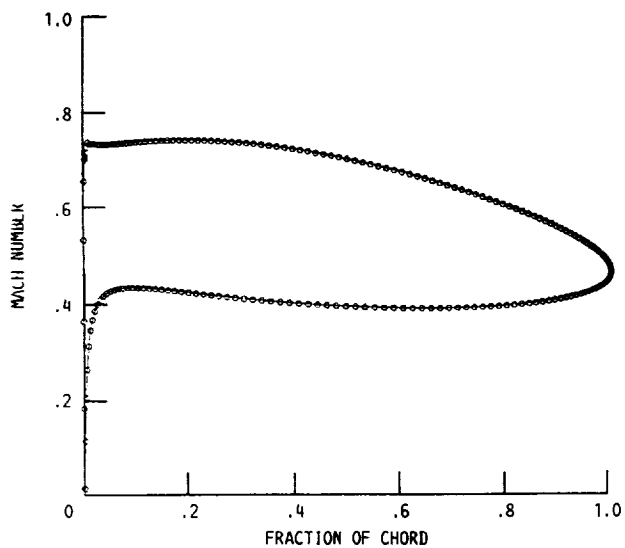
FIGURE 6. - MEAN FLOW MACH NUMBER AT THE AIRFOIL SURFACE FOR A 6 PERCENT THICK JOUKOWSKI AIRFOIL WITH M_∞ = .5, α = 2°, AND CAMBER RATIO = 0.05. STEADY C_L = 1.05. CALCULATION BY FLO36.
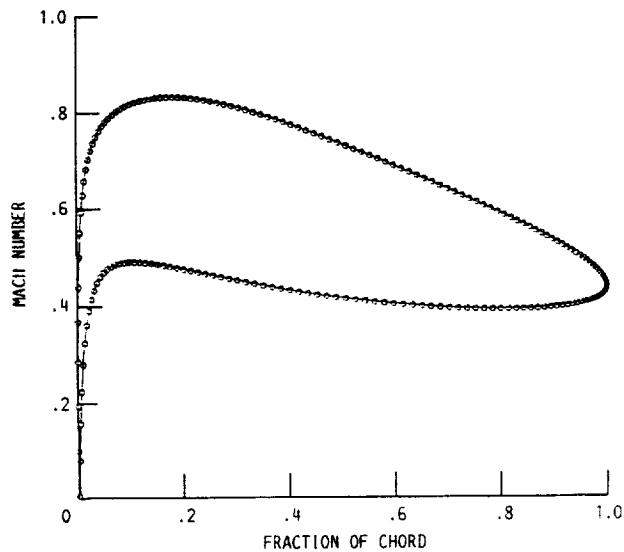
FIGURE 7. - MEAN FLOW MACH NUMBER AT THE AIRFOIL SURFACE FOR A 12 PERCENT THICK JOUKOWSKI AIRFOIL WITH M_∞ = .5, α = 2°, AND CAMBER RATIO = 0.05. STEADY C_L = 1.11. CALCULATION BY FLO36.

14
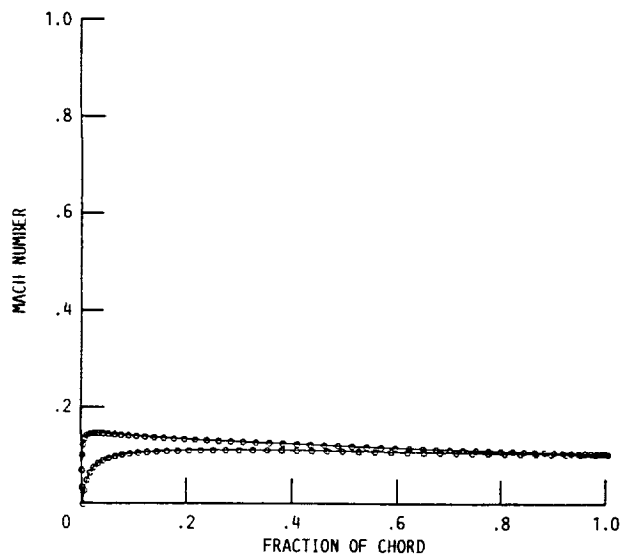
FIGURE 8. - MEAN FLOW MACH NUMBER AT THE AIRFOIL SURFACE FOR A 12 PERCENT THICK JOUKOWSKI AIRFOIL WITH M_∞ = .1, α = 3°, AND CAMBER RATIO = 0.0. STEADY C_L = 0.36.

FIGURE 9. - MEAN FLOW MACH NUMBER AT THE AIRFOIL SURFACE FOR A 12 PERCENT THICK JOUKOWSKI AIRFOIL WITH M_∞= .6, α = 3°, AND CAMBER RATIO = 0.0. STEADY C_L = 0.48. CALCULATION BY FLO36.
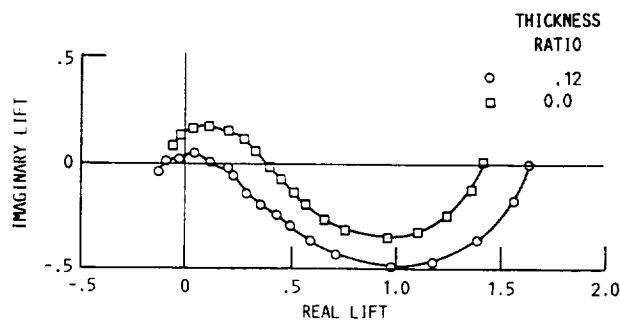
FIGURE 10. - EFFECT OF THICKNESS ON THE UNSTEADY LIFT OF A SYMMETRIC JOUKOWSKI AIRFOIL IN A TRANSVERSE GUST. M_∞ = .7, α = 0°, CAMBER RATIO = 0.0.
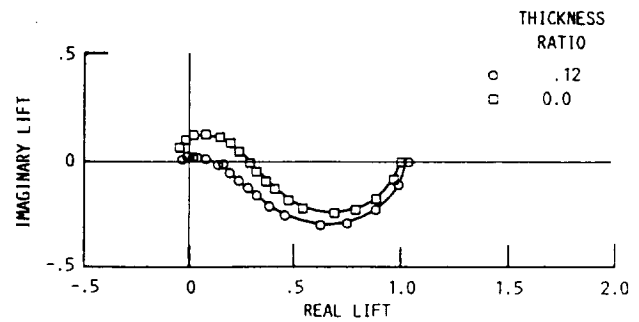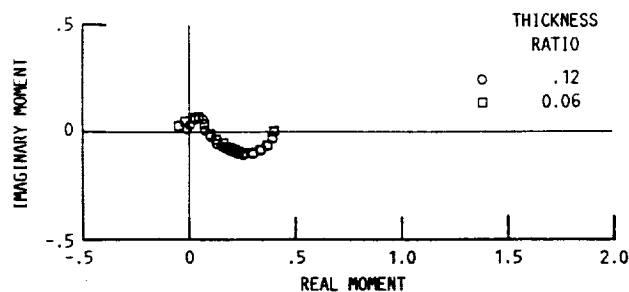

FIGURE 11. - EFFECT OF THICKNESS ON THE UNSTEADY LIFT OF A SYMMETRIC JOUKOWSKI AIRFOIL IN A TRANSVERSE AND LONGITUDINAL GUST. M_∞ = .7, α = 0°, CAMBER RATIO = 0.0.
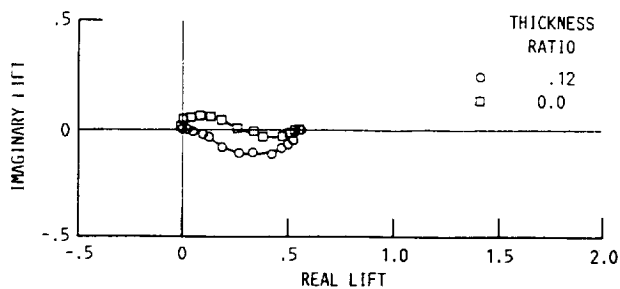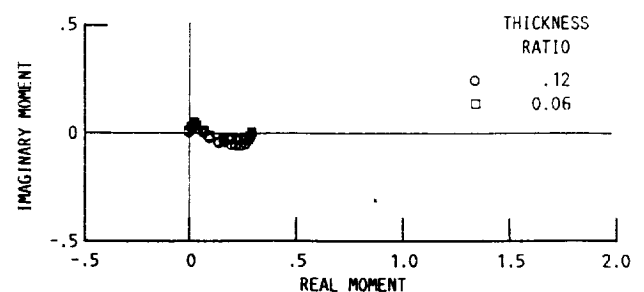

FIGURE 12. - EFFECT OF THICKNESS ON THE UNSTEADY LIFT OF A SYMMETRIC JOUKOWSKI AIRFOIL IN A THREE-DIMENSIONAL GUST. M_∞ = .7, α = 0°, CAMBER RATIO = 0.0.
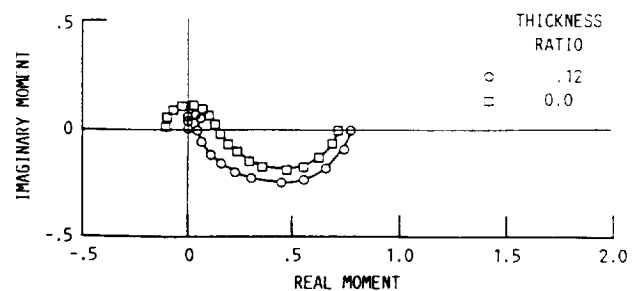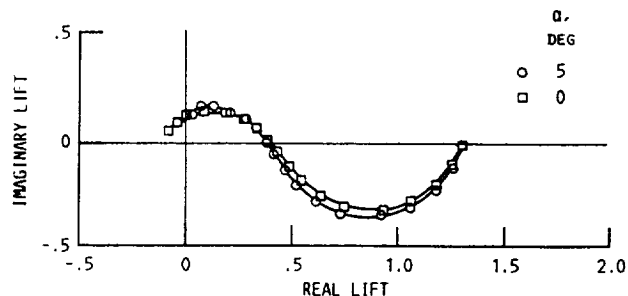

FIGURE 13. - EFFECT OF THICKNESS ON THE UNSTEADY MOMENT OF A SYMMETRIC JOUKOWSKI AIRFOIL IN A TRANSVERSE GUST. M_∞ = .7, α = 0°, CAMBER RATIO = 0.0.

15
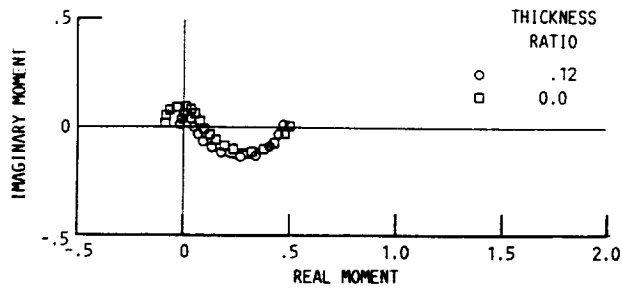
FIGURE 14. - EFFECT OF THICKNESS ON THE UNSTEADY MOMENT
OF A SYMMETRIC JOUKOWSKI AIRFOIL IN A TRANSVERSE AND
LONGITUDINAL GUST. M_∞ = .7, α = 0^0, CAMBER RATIO =
0.0.
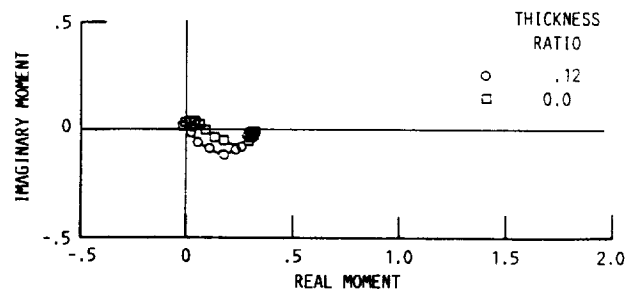
FIGURE 15. - EFFECT OF THICKNESS ON THE UNSTEADY MOMENT
OF A SYMMETRIC JOUKOWSKI AIRFOIL IN A THREE-DIMENSIONAL
GUST. M_∞ = .7, α = 0^0, CAMBER RATIO = 0.0.
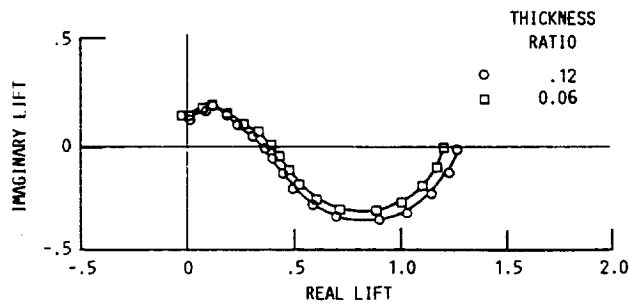
FIGURE 16. - EFFECT OF THICKNESS ON THE UNSTEADY LIFT OF
A JOUKOWSKI AIRFOIL IN A TRANSVERSE GUST. M_∞ = .5,
α = 2^0, CAMBER RATIO = 0.05.
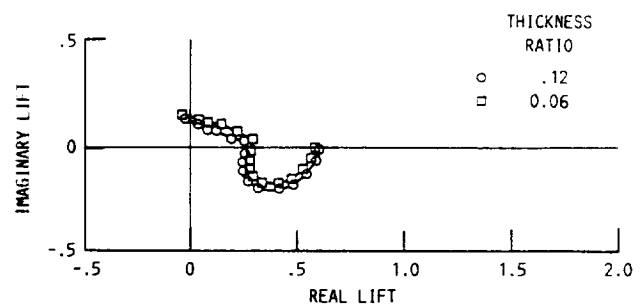
FIGURE 17. - EFFECT OF THICKNESS ON THE UNSTEADY LIFT OF
A JOUKOWSKI AIRFOIL IN A TRANSVERSE AND LONGITUDINAL
GUST. M_∞ = .5, α = 2^0, CAMBER RATIO = 0.05.
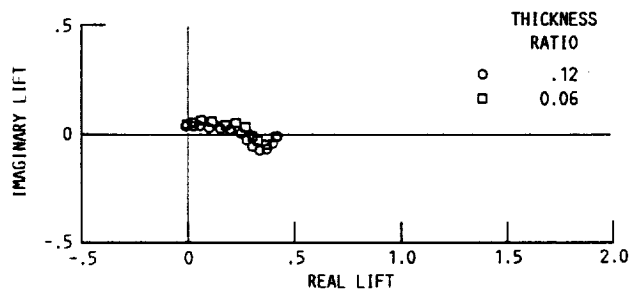
FIGURE 18. - EFFECT OF THICKNESS ON THE UNSTEADY LIFT OF A
JOUKOWSKI AIRFOIL IN A THREE-DIMENSIONAL GUST. M_∞ = .5,
α = 2^0, CAMBER RATIO = 0.05.
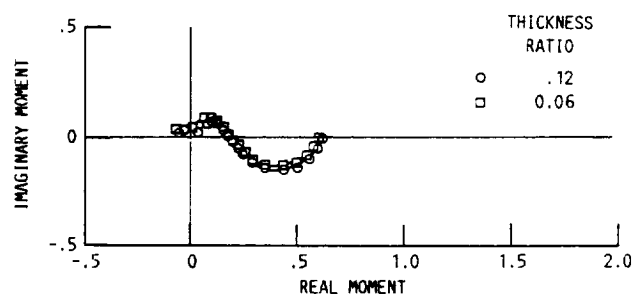
FIGURE 19. - EFFECT OF THICKNESS ON THE UNSTEADY MOMENT
OF A JOUKOWSKI AIRFOIL IN A TRANSVERSE GUST, M_∞ = .5,
α = 2^0, CAMBER RATIO = 0.05.

FIGURE 20. - EFFECT OF THICKNESS ON THE UNSTEADY MOMENT OF
A JOUKOWSKI AIRFOIL IN A TRANSVERSE AND LONGITUDINAL GUST.
M_∞ = .5, α = 2^0, CAMBER RATIO = 0.05.

FIGURE 21. - EFFECT OF THICKNESS ON THE UNSTEADY MOMENT
OF A JOUKOWSKI AIRFOIL IN A THREE-DIMENSIONAL GUST.
M_∞ = .5, α = 2^0, CAMBER RATIO = 0.05.

FIGURE 22. - EFFECT OF ANGLE OF ATTACK ON THE UNSTEADY
LIFT OF A SYMMETRIC JOUKOWSKI AIRFOIL IN A TRANSVERSE
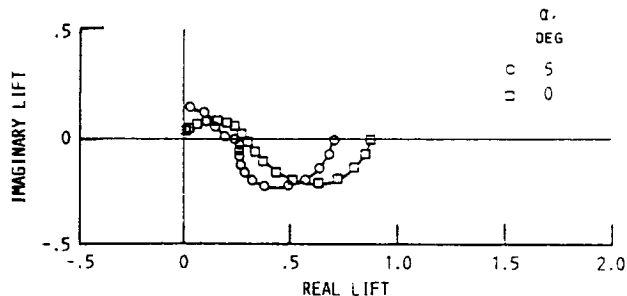GUST. M_∞ = .5, THICKNESS RATIO = .12, CAMBER RATIO =
0.0.

FIGURE 23. - EFFECT OF ANGLE OF ATTACK ON THE UNSTEADY
LIFT OF A SYMMETRIC JOUKOWSKI AIRFOIL IN A TRANSVERSE
AND LONGITUDINAL GUST. M_∞ = .5, THICKNESS RATIO =
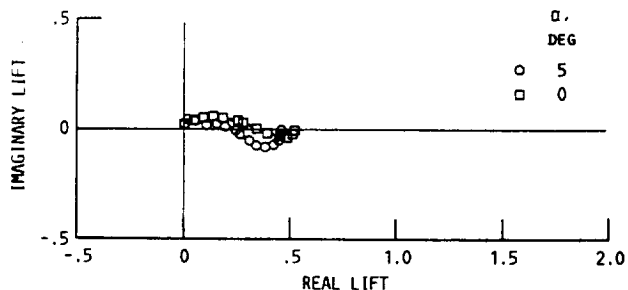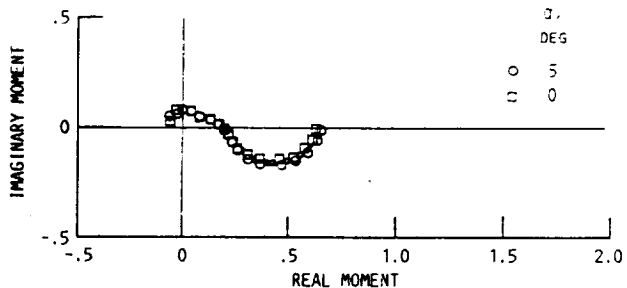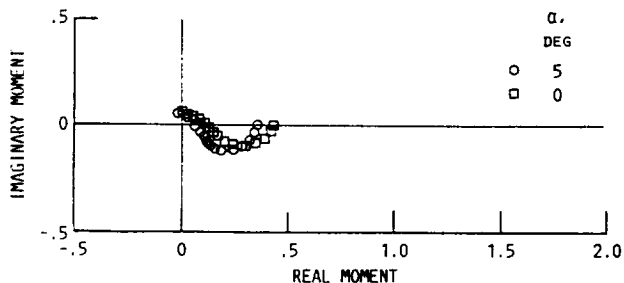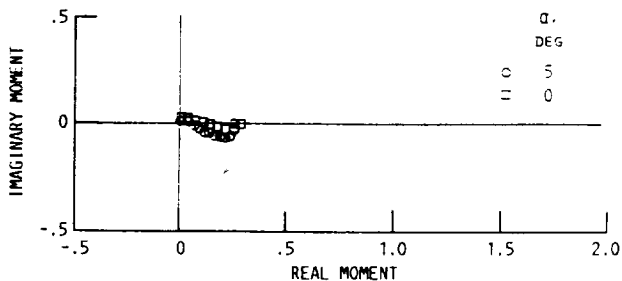.12, CAMBER RATIO = 0.0.

FIGURE 24. - EFFECT OF ANGLE OF ATTACK ON THE UNSTEADY
LIFT OF A SYMMETRIC JOUKOWSKI AIRFOIL IN A THREE-
DIMENSIONAL GUST. M_∞ = .5, THICKNESS RATIO = .12,
CAMBER RATIO = 0.0.

FIGURE 25. - EFFECT OF ANGLE OF ATTACK ON THE UNSTEADY
MOMENT OF A SYMMETRIC JOUKOWSKI AIRFOIL IN A TRANS-
VERSE GUST. M_∞ = .5, THICKNESS RATIO = .12, CAMBER
RATIO = 0.0.

FIGURE 26. - EFFECT OF ANGLE OF ATTACK ON THE UNSTEADY
MOMENT OF A SYMMETRIC JOUKOWSKI AIRFOIL IN A TRANS-
VERSE AND LONGITUDINAL GUST. M_∞ = .5, THICKNESS
RATIO = .12, CAMBER RATIO = 0.0.

FIGURE 27. - EFFECT OF ANGLE OF ATTACK ON THE UNSTEADY
MOMENT OF A SYMMETRIC JOUKOWSKI AIRFOIL IN A THREE-
DIMENSIONAL GUST. M_∞ = .5, THICKNESS RATIO = .12,
CAMBER RATIO = 0.0.

17

CAMBER
RATIO
○ .05
□ 0

IMAGINARY LIFT
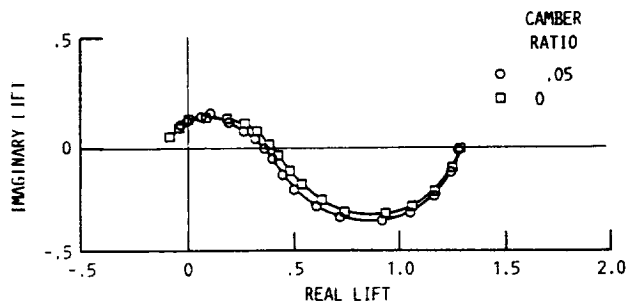
.5

0

-.5

REAL LIFT

-.5   0   .5   1.0   1.5   2.0

FIGURE 28. - EFFECT OF CAMBER ON THE UNSTEADY LIFT OF A
JOUKOWSKI AIRFOIL IN A TRANSVERSE GUST. M_∞ = .5,
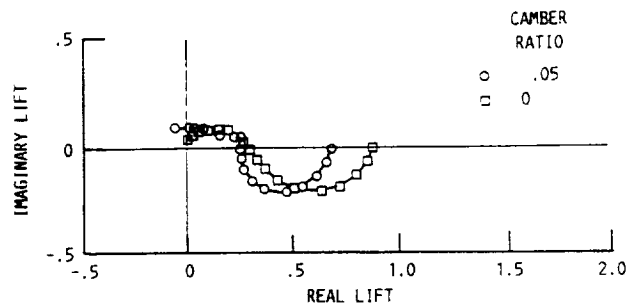α = 0^0, THICKNESS RATIO = .12.

CAMBER
RATIO
○ .05
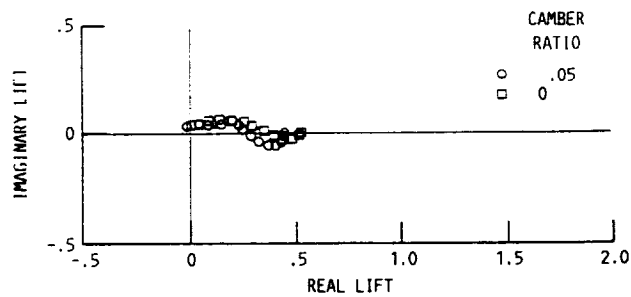□ 0

IMAGINARY LIFT

.5

0

-.5

REAL LIFT

-.5   0   .5   1.0   1.5   2.0

FIGURE 29. - EFFECT OF CAMBER ON THE UNSTEADY LIFT OF A
JOUKOWSKI AIRFOIL IN A TRANSVERSE AND LONGITUDINAL GUST.
M_∞ = .5, α = 0^0, THICKNESS RATIO = .12.

CAMBER
RATIO
○ .05
□ 0

IMAGINARY LIFT

.5

0

-.5

REAL LIFT

-.5   0   .5   1.0   1.5   2.0

FIGURE 30. - EFFECT OF CAMBER ON THE UNSTEADY LIFT OF A
JOUKOWSKI AIRFOIL IN A THREE-DIMENSIONAL GUST. M_∞ =
.5, α = 0^0, THICKNESS RATIO = .12.

CAMBER
RATIO
○ .05
□ 0

IMAGINARY MOMENT

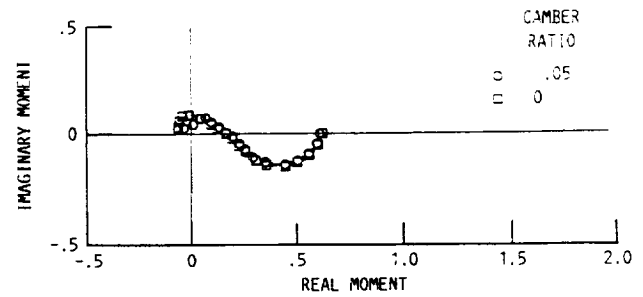.5

0

-.5

REAL MOMENT

-.5   0   .5   1.0   1.5   2.0

FIGURE 31. - EFFECT OF CAMBER ON THE UNSTEADY MOMENT OF
A JOUKOWSKI AIRFOIL IN A TRANSVERSE GUST. M_∞ = .5,
α = 0^0, THICKNESS RATIO = .12.

CAMBER
RATIO
○ .05
□ 0

IMAGINARY MOMENT

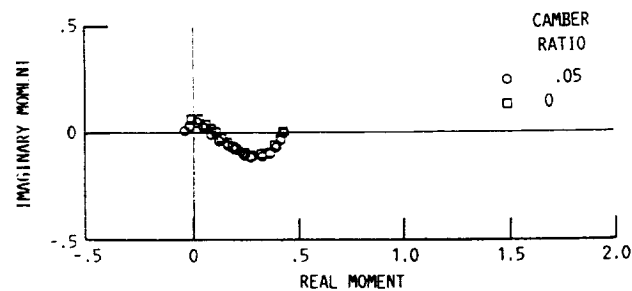.5

0

-.5

REAL MOMENT

-.5   0   .5   1.0   1.5   2.0

FIGURE 32. - EFFECT OF CAMBER ON THE UNSTEADY MOMENT OF
A JOUKOWSKI AIRFOIL IN A TRANSVERSE AND LONGITUDINAL
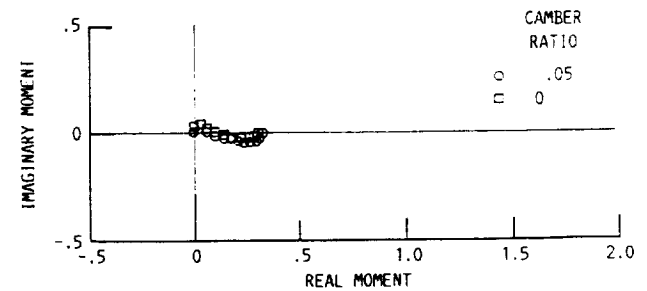GUST. M_∞ = .5, α = 0^0, THICKNESS RATIO = .12.

CAMBER
RATIO
○ .05
□ 0

IMAGINARY MOMENT

.5

0

-.5

REAL MOMENT

-.5   0   .5   1.0   1.5   2.0

FIGURE 33. - EFFECT OF CAMBER ON THE UNSTEADY MOMENT OF A
JOUKOWSKI AIRFOIL IN A THREE-DIMENSIONAL GUST. M_∞ = .5,
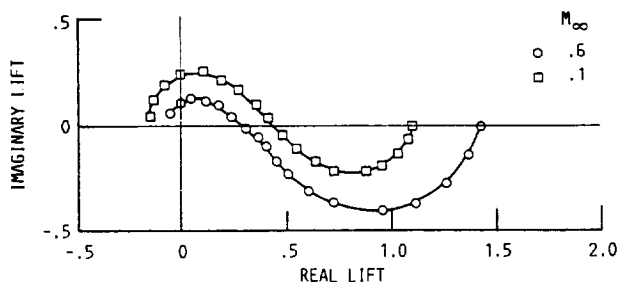α = 0^0, THICKNESS RATIO = .12.

FIGURE 34. - EFFECT OF MACH NUMBER ON THE UNSTEADY LIFT
OF A SYMMETRIC JOUKOWSKI AIRFOIL IN A TRNASVERSE GUST.
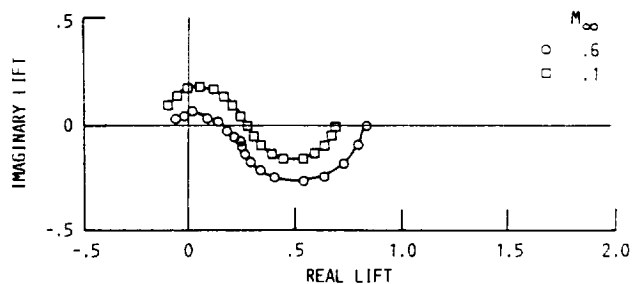α = 3°, CAMBER RATIO = 0.0, THICKNESS RATIO = .12.

FIGURE 35. - EFFECT OF MACH NUMBER ON THE UNSTEADY LIFT
OF A SYMMETRIC JOUKOWSKI AIRFOIL IN A TRANSVERSE AND
LONGITUDINAL GUST. α = 3°, CAMBER RATIO = 0.0, THICK-
NESS RATIO = .12.
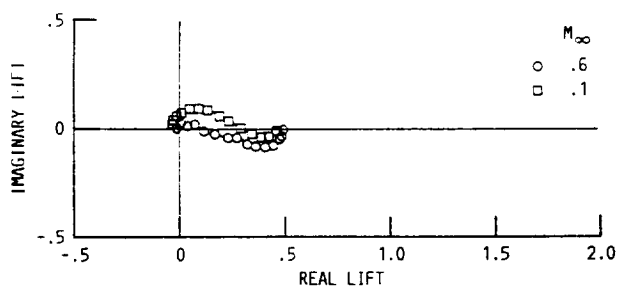

FIGURE 36. - EFFECT OF MACH NUMBER ON THE UNSTEADY LIFT
OF A SYMMETRIC JOUKOWSKI AIRFOIL IN A THREE-DIMENSIONAL
GUST. α = 3°, CAMBER RATIO = 0.0, THICKNESS RATIO =
.12.

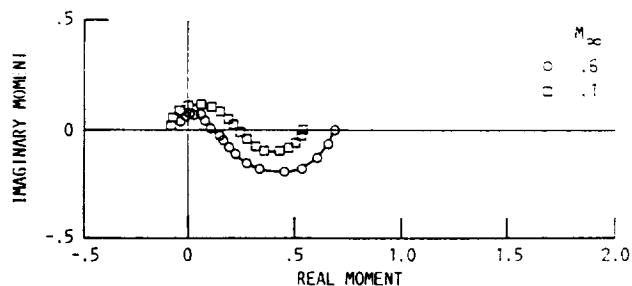FIGURE 37. - EFFECT OF MACH NUMBER ON THE UNSTEADY
MOMENT OF A SYMEMTRIC JOUKOWSKI AIRFOIL IN A TRANS-
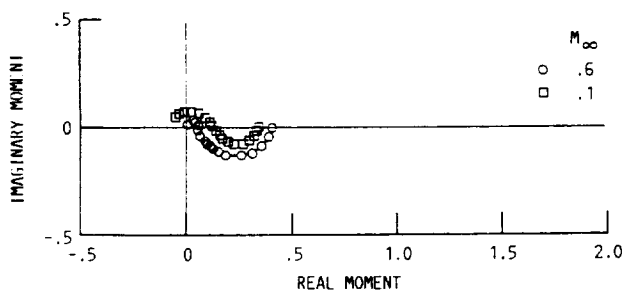VERSE GUST. α = 3°, CAMBER RATIO = 0.0, THICKNESS
RATIO = .12.

FIGURE 38. - EFFECT OF MACH NUMBER ON THE UNSTEADY MOMENT
OF A SYMMETRIC JOUKOWSKI AIRFOIL IN A TRANSVERSE AND
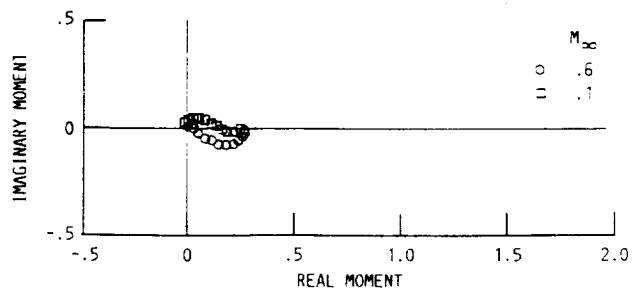LONGITUDINAL GUST. α = 3°, CAMBER RATIO = 0.0, THICK-
NESS RATIO = .12.

FIGURE 39. - EFFECT OF MACH NUMBER ON THE UNSTEADY MO-
MENT OF A SYMMETRIC JOUKOWSKI AIRFOIL IN A THREE-
DIMENSIONAL GUST. α = 3°, CAMBER RATIO = 0.0, THICK-
NESS RATIO = .12.

19

Report Documentation Page

1. Report No. NASA TM-102466 AIAA-90-0694	2. Government Accession No.	3. Recipient's Catalog No.
4. Title and Subtitle Numerical Solutions of the Linearized Euler Equations for Unsteady Vortical Flows Around Lifting Airfoils		5. Report Date
		6. Performing Organization Code
7. Author(s) James R. Scott and Hafiz M. Atassi		8. Performing Organization Report No. E-5137
		10. Work Unit No. 505-62-21
9. Performing Organization Name and Address National Aeronautics and Space Administration Lewis Research Center Cleveland, Ohio 44135-3191		11. Contract or Grant No.
		13. Type of Report and Period Covered Technical Memorandum
12. Sponsoring Agency Name and Address National Aeronautics and Space Administration Washington, D.C. 20546-0001		14. Sponsoring Agency Code

15. Supplementary Notes

Prepared for the 28th Aerospace Sciences Meeting sponsored by the American Institute of Aeronautics and Astronautics, Reno, Nevada, January 8-11, 1990. James R. Scott, NASA Lewis Research Center; Hafiz M. Atassi, University of Notre Dame, Notre Dame, Indiana 46556.

16. Abstract

A linearized unsteady aerodynamic analysis is presented for unsteady, subsonic vortical flows around lifting airfoils. The analysis fully accounts for the distortion effects of the nonuniform mean flow on the imposed vortical disturbances. A frequency domain numerical scheme which implements this linearized approach is described, and numerical results are presented for a large variety of flow configurations. The results demonstrate the effects of airfoil thickness, angle of attack, camber, and Mach number on the unsteady lift and moment of airfoils subjected to periodic vortical gusts. The results show that mean flow distortion can have a very strong effect on the airfoil unsteady response, and that the effect depends strongly upon the reduced frequency, Mach number, and gust wave numbers.

17. Key Words (Suggested by Author(s)) Unsteady; Vertical; Euler equations; Airfoils; Numerical; Linearized; Rapid distortion	18. Distribution Statement Unclassified – Unlimited Subject Category 02		
19. Security Classif. (of this report) Unclassified	20. Security Classif. (of this page) Unclassified	21. No. of pages	22. Price*

NASA FORM 1626 OCT 86   *For sale by the National Technical Information Service, Springfield, Virginia 22161